The impact of phage and phage resistance on microbial community dynamics

Ellinor O Alseth[1,2,3¶*], Rafael Custodio[1¶], Sarah A Sundius[2,4,5], Rachel A Kuske[2,4], Sam P. Brown[2,3&], Edze R Westra[1&]

[1]Environment and Sustainability Institute, Biosciences, University of Exeter, Penryn, UK

[2]Center for Microbial Dynamics and Infection, Georgia Institute of Technology, Atlanta, Georgia, USA

[3]School of Biological Sciences, Georgia Institute of Technology, Atlanta, Georgia, USA

[4]School of Math, Georgia Institute of Technology, Atlanta, Georgia, USA

[5]Interdisciplinary Program in Quantitative Biosciences, Georgia Institute of Technology, Atlanta, Georgia, USA

* Corresponding author

E-mail: ealseth3@gatech.edu (EOA)

¶ These authors contributed equally to this work.

& These authors also contributed equally to this work.

Abstract

Where there are bacteria, there will be bacteriophages. These viruses are known to be important players in shaping the wider microbial community in which they are embedded, with potential implications for human health. On the other hand, bacteria possess a range of distinct immune mechanisms that provide protection against bacteriophages, including the mutation or complete loss of the phage receptor, and CRISPR-Cas adaptive immunity. Yet little is known about how interactions between phages and these different phage resistance mechanisms affect the wider microbial community in which they are embedded. Here, we conducted a 10-day, fully factorial evolution experiment to examine how phage impact the structure and dynamics of an artificial four-species bacterial community that includes either *Pseudomonas aeruginosa* wild type or an isogenic mutant unable to evolve phage resistance through CRISPR-Cas. Our results show that the microbial community structure is drastically altered by the addition of phage, with *Acinetobacter baumannii* becoming the dominant species and *P. aeruginosa* being driven nearly extinct, whereas *P. aeruginosa* outcompetes the other species in the absence of phage. Moreover, we find that a *P. aeruginosa* strain with the ability to evolve CRISPR-based resistance generally does better when in the presence of *A. baumannii*, but that this benefit is largely lost over time as phage is driven extinct. Combined, our data highlight how phage-targeting a dominant species allows for the competitive release of the strongest competitor whilst also contributing to community diversity maintenance and potentially preventing the reinvasion of the target species, and underline the importance of mapping community composition before therapeutically applying phage.

Introduction

Microbiome research is a dynamic and growing field in microbiology, producing an incredible amount of sequence data from a wide range of clinical and environmental samples. Humans, for instance, are colonised by a large number of microorganisms and research continues to implicate microbial communities as potential drivers behind multiple important biological processes [1–3]. These processes may play important roles in human health and disease, with some work focusing on correlations based on microbiome composition [4–8] while other look more closely for direct causality [9–12]. Still, the challenge to move beyond descriptive and correlative approaches remains, and there is a need to develop bottom-up mechanistic and quantitative understanding of the forces acting upon and shaping microbial communities. To this end, synthetic polymicrobial communities are being designed, and are gaining traction in both pure and applied microbiome studies [13–16]. Synthetic microbiomes allow for precise and malleable experimental testing of the basic rules that govern both microbial organisation and functioning on molecular and ecological scales [17–20], as well as allowing for exploration of causal roles connecting specific microbiome structures to potential outcomes of interest.

Bacteria and their viral predators, bacteriophages (phages), have long been of interest in microbiological research, in part due to being the most abundant biological entity on the planet [21,22]. Phages are highly diverse in terms of their morphology, genetics, and life histories [21,23], with a clear distinction between obligatory killing lytic phages and temperate phages that can either cause a dormant infection (lysogenic cycle) or cell lysis

to release new phage particles (lytic cycle). Phages are thought to play a key role in shaping both the taxonomic and functional composition of microbial communities as well as their stability, ecology and evolution [23–26]. For example, lytic replication will per definition cause a reduction in the density of the bacterial host strain or species, which in turn can have knock-on effects for the microbial community composition through the enabling of invasion and/or co-existence of competitor species. Despite the large potential impact of lytic phage, only a very limited number of experimental studies have explored the ecology and evolution of bacteria-phage interactions in a microbial community context [27,28], and it remains unclear if and how interactions between different species in more complex communities shape the effects of lytic phages on microbial eco-evolutionary dynamics. Consequently, we lack the steppingstones to understand how phages shape microbial community dynamics (reviewed in [23]), which are urgently needed to understand potentially causal relationships between natural phage communities and a variety of human diseases [29–34], and for optimising the therapeutic application of phages in the clinic .

A key consideration in this context is that bacteria can overcome phage infection through a range of different means [35,36], with varied underlying molecular mechanisms and which can act during different stages of phage infection [37–40]. Through the modification, masking or complete loss of phage-binding surface receptors for example, bacteria can prevent phage adsorption and injection [39,41]. Systems such as CRISPR-Cas on the other hand work by inserting short DNA sequences from phage and other invasive mobile genetic elements into the host genome to provide future immunological

memory [42]. Unlike CRISPR-based resistance [15], phage resistance through receptor mutation can be associated with substantial phenotypic shifts and fitness trade-offs, through changes to virulence [43,44], biofilm formation [45], or antibiotic resistance [46].

Combining an exploratory and hypothesis driven approach, we applied experimental evolution to examine how a phage impacts the dynamics of an artificial bacterial community. This community consisted of *Pseudomonas aeruginosa*, *Staphylococcus aureus, Acinetobacter baumannii*, and *Burkholderia cenocepacia*, all of which are opportunistic pathogens that can cause severe infection and may co-infect with one another [47–50]. Firstly, we hypothesised that the addition of a *P. aeruginosa* specific phage would promote species coexistence by limiting *P. aeruginosa* dominance through competitive release (expansion of phage resistant competitors, following removal of phage susceptible competitor) in a way akin to what is commonly observed with antibiotics [14,51–54]. Secondly, we hypothesised that blocking the ability of *P. aeruginosa* to evolve CRISPR-based immunity would reduce *P. aeruginosa* persistence due to community dependent fitness costs of surface-modification [15]. We found that the addition of a *P. aeruginosa* targeting phage resulted in the general maintenance of community diversity and coexistence, but also a shift in dominant species from *P. aeruginosa* to *A. baumannii* – with the former being unable to reinvade even after the phage was driven extinct. The impact of the type of phage resistance was limited or transient, however: While a *P. aeruginosa* wild-type with the ability to evolve CRISPR-based phage resistance initially had a slight fitness advantage in the presence of *A.*

110 *baumannii* over its CRISPR-negative isogenic mutant, this effect was lost over time as
111 the phage was driven extinct.
112

113 Results

114 To measure the effect of phage on microbial community dynamics, we carried out a fully
115 factorial 10-day *in vitro* evolution experiment using all possible combinations of one, two,
116 three or four competitor species: *S. aureus*, *A. baumannii*, *B. cenocepacia*, and *P.*
117 *aeruginosa* PA14 in the presence or absence of lytic phage DMS3vir. Additionally, to
118 examine the impact of CRISPR-Cas vs surface modification on these dynamics, we used
119 both the wild-type (WT) *P. aeruginosa* PA14 strain, which can evolve CRISPR-based
120 phage resistance and an isogenic mutant lacking a functional CRISPR system. Following
121 inoculation, we tracked the microbial community dynamics for all experimental treatments
122 at regular intervals over a period of 10 days. All experiments were conducted in Lysogeny
123 Broth (LB) at 37˚C (see methods for details).
124

125 *P. aeruginosa* dominates in the absence of phage

126 Without *P. aeruginosa* present in the community, *S. aureus* was primarily the dominant
127 species – with the ability to co-exist with *A. baumannii* while outcompeting *B. cenocepacia*
128 (Figs 1 and S1). This, however, was not reflected once *P. aeruginosa* was introduced to
129 the community. In the absence of phage, *P. aeruginosa* quickly became the dominant
130 species in the microbial community, regardless of starting composition and the *P.*
131 *aeruginosa* genotype (PA14 WT vs CRISPR-KO) (Figs 2 and S3). Consistent with this,
132 the densities of the competitor species rapidly declined during these co-culture

133 experiments (Fig 2). Yet there was a clear difference in the rate at which competitor
134 species declined in frequency, which was highest for *S. aureus* and lowest for *A.*
135 *baumannii* (Fig 2, ANOVA: effect of treatment on *S. aureus*; F = 2.2, p = 0.09 ; overall
136 model fit; adjusted R^2 = 0.60, $F_{20,171}$ = 15.45, p < 2.2 x 10^{-16}: effect of treatment on *A.*
137 *baumannii*; F = 0.52, p = 0.67; overall model fit; adjusted R^2 = 0.66, $F_{20,171}$ = 19.89, p <
138 2.2 x 10^{-16}: effect of treatment on *B. cenocepacia*; F = 1.36, p = 0.26; overall model fit;
139 adjusted R^2 = 0.69, $F_{20,171}$ = 22.45, p < 2.2 x 10^{-16}).

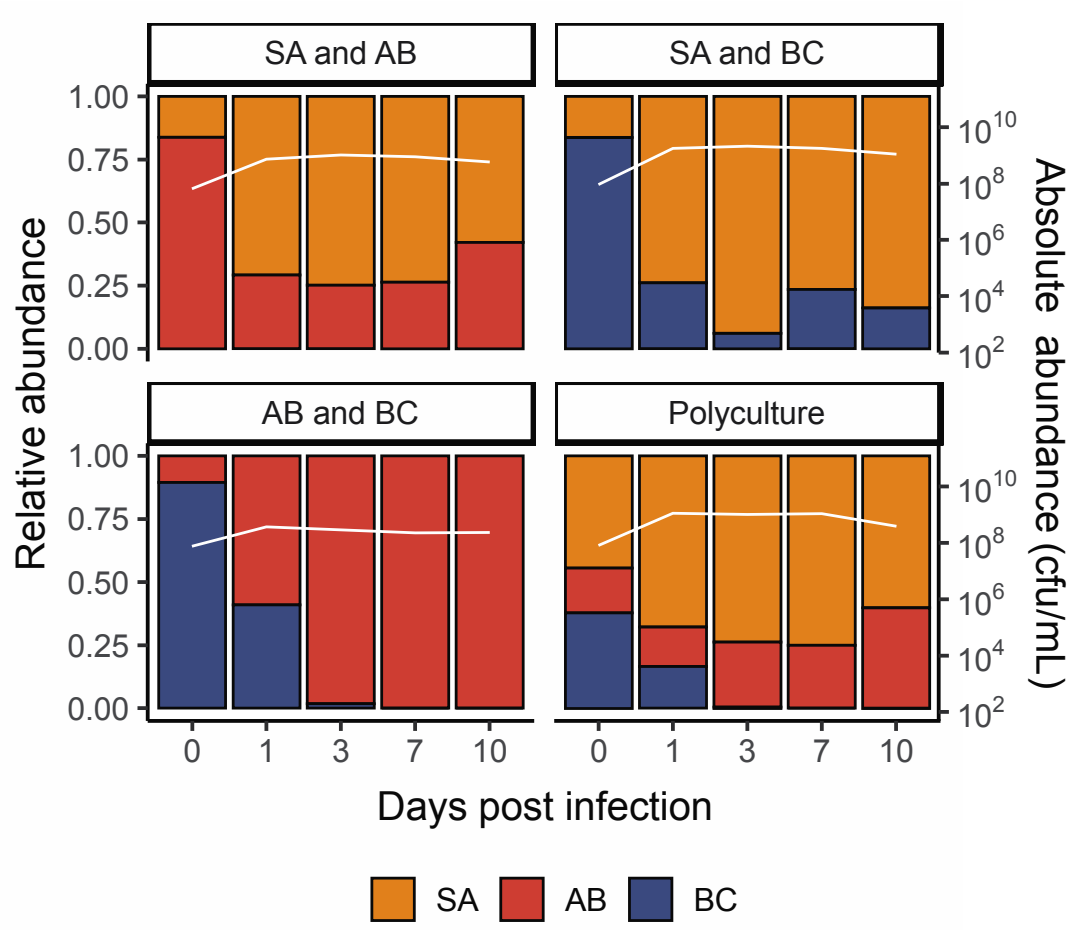

140

141 **Fig 1. *S. aureus* and *A. baumannii* both perform well in the absence of P.**
142 **aeruginosa.** Showing the community composition and bacterial densities in cfu/mL over
143 time for the microbial communities in the absence of *P. aeruginosa*. The community

144 composition was estimated by qPCR at days 0, 1, 3, 7 and 10 of the experiment. The
145 coloured bars represent the relative abundance of each species (left y axis), while the
146 white line represents total abundance in cfu/mL (right y axis). Each panel represents
147 average composition across six replicates for each treatment over time. SA = *S. aureus*,
148 AB = *A. baumannii*, BC = *B. cenocepacia*. For individual replicates of species abundance,
149 see Fig. S1.

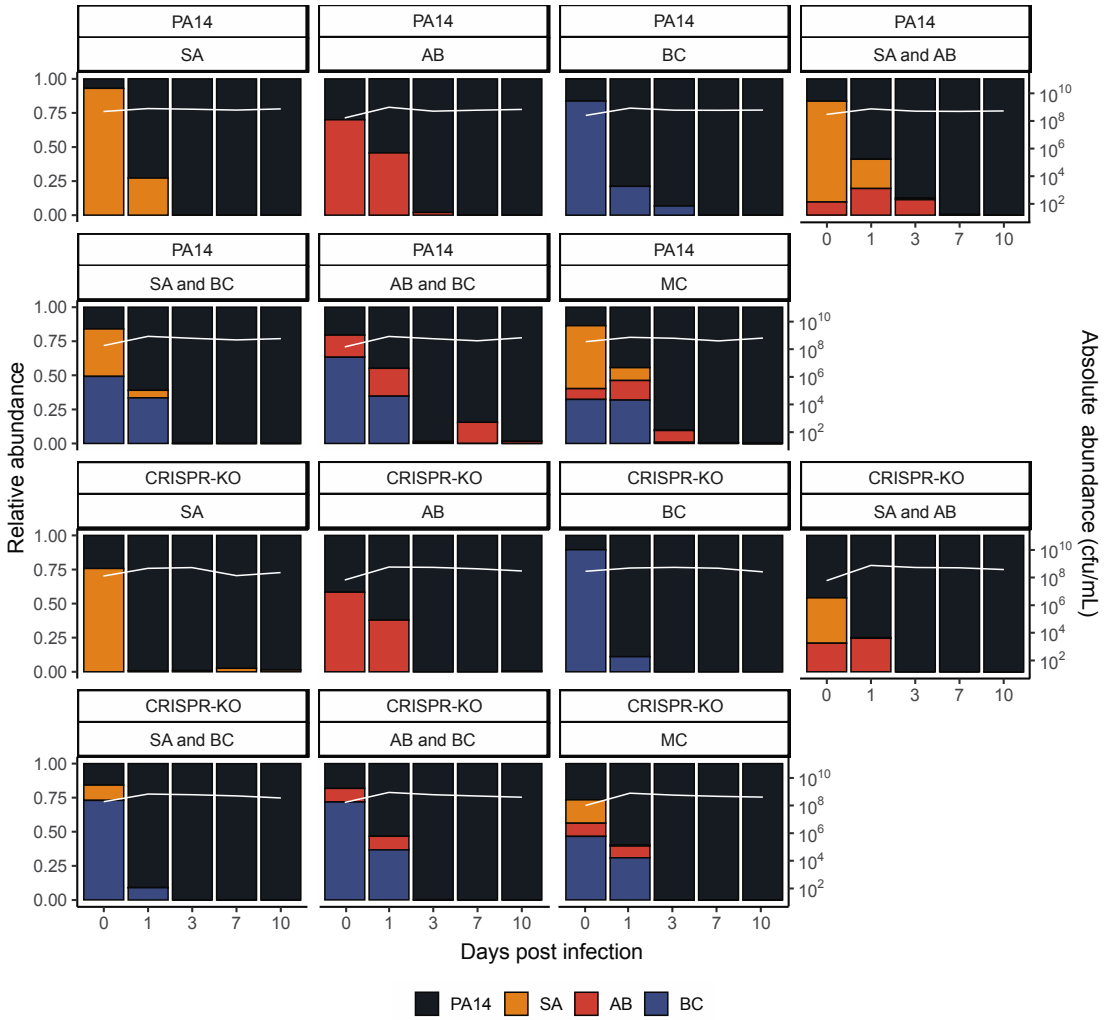

150

151 **Fig 2. *Pseudomonas aeruginosa* becomes the dominant species in the absence of**
152 **phage.** Showing the community composition and bacterial densities in cfu/mL over time
153 for the microbial communities in the absence of phage. The community composition was

154 estimated by qPCR at days 0, 1, 3, 7 and 10 of the experiment. The coloured bars
155 represent the relative abundance of each species (left y axis), while the white line
156 represents total abundance in cfu/mL (right y axis). Each panel represents average
157 composition across six replicates for each treatment over time. PA14 = *P. aeruginosa*,
158 SA = *S. aureus*, AB = *A. baumannii*, BC = *B. cenocepacia*, MC = microbial community.
159 For individual replicates of species abundance, see Fig. S3.
160
161 While the microbial community dynamics were relatively similar for the WT and CRISPR-
162 KO strains, some significant differences were observed. For example, the densities of the
163 CRISPR-KO strain were slightly lower in the presence compared to the absence of *S.*
164 *aureus* on its own (Fig 2, linear model: $t = 2.048$, $p = 0.0413$; overall model fit; adjusted
165 $R^2 = 0.21$, $F_{36,345} = 3.77$, $p < 6.03 \times 10^{-11}$). Moreover, *S. aureus* and *A. baumannii* reached
166 higher densities in the presence of the PA14 WT compared to the CRISPR-KO strain,
167 particularly at the earlier timepoints (Fig 2). In contrast to this, densities of *B. cenocepacia*
168 over time were similar in the presence of both *P. aeruginosa* genotypes (Fig 2).
169 Regardless these minor differences, *P. aeruginosa* consistently and readily outcompeted
170 the other community members in the absence of phage, with all three being extinct or
171 close to extinction by day 10 (Fig 2). For visualisation purposes, the data from Figure 2 is
172 also presented as an ordination plot (Fig S2).
173

174 Phage affects microbial community dynamics

175 Whereas *P. aeruginosa* dominated in the absence of phage, we hypothesised this would
176 change once a PA14 targeting phage (DMS3vir) was introduced, largely by a virulent

177 phage reducing the susceptible host population, facilitating expansion of other species
178 through competitive release [14,51–54]. As expected, phage DMS3vir initially reached
179 high titres due to replication on sensitive *P. aeruginosa* hosts, followed by a rapid decline
180 in phage densities due to the evolution of phage resistance, regardless of whether the
181 host had a functional CRISPR-Cas system or not (Fig S4). Crucially however, the
182 presence of phage caused microbial communities to no longer be dominated by *P.*
183 *aeruginosa*, as when compared to the no phage treatments, very few to none of the
184 experimental repeats had one or more bacterial species go extinct, with *A. baumannii*
185 reaching particularly high abundance (Figs 3 and S5). It is here worth noting that while *B.*
186 *cenocepacia* is not visible at later timepoints in the compositional plot due to low relative
187 abundance of <0.1 (Fig 3), we consistently observed persistence of *B. cenocepacia* at an
188 average of ~10^4 cfu/mL across all treatments (see Fig S5). For visualisation purposes,
189 the data from Figure 3 is also presented as an ordination plot (Fig S6).

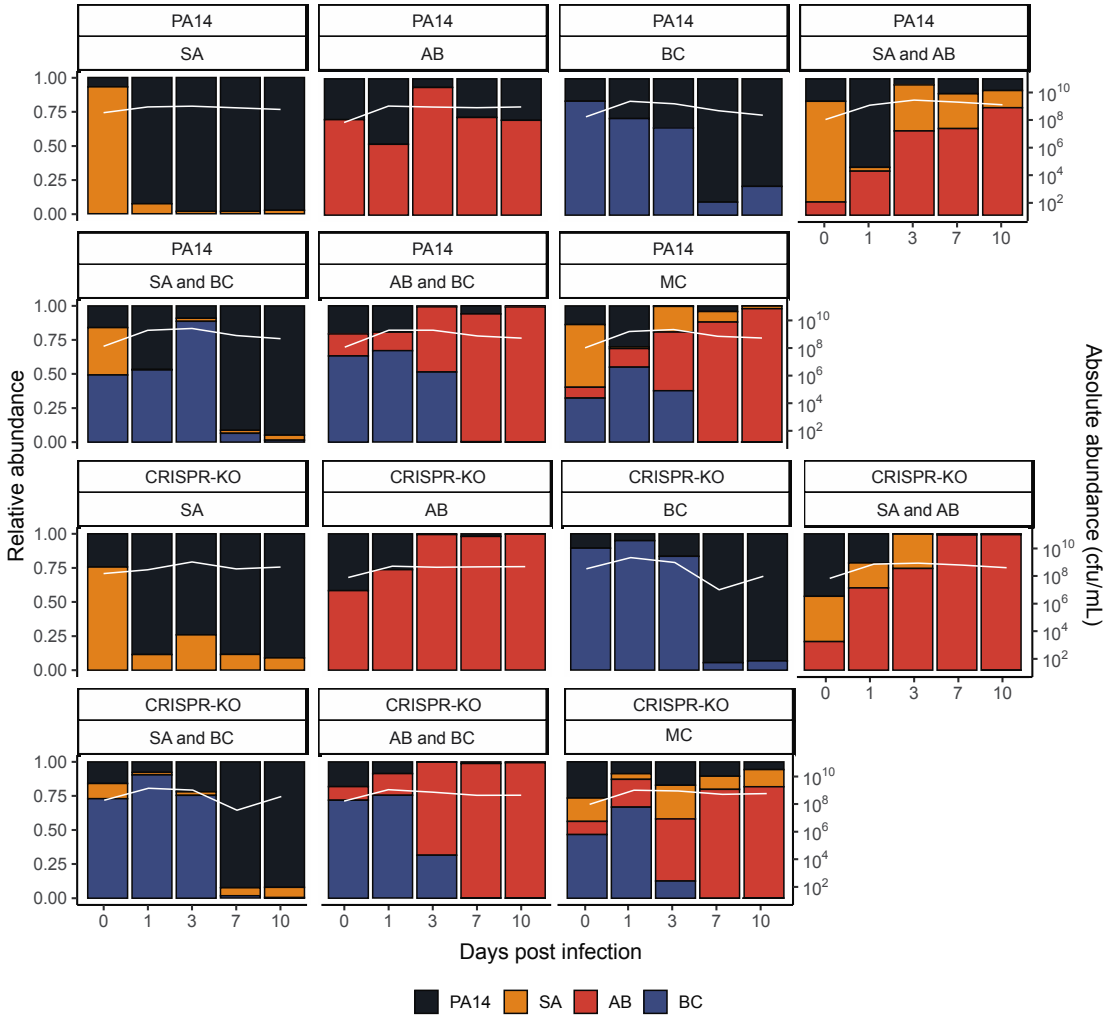

Fig 3. Phage allows for the maintenance of all microbial community members, with *A. baumannii* becoming the new dominant species. Showing the community composition and bacterial densities in cfu/mL over time for the microbial communities in the presence of phage. The community composition was estimated by qPCR at days 0, 1, 3, 7 and 10 of the experiment. The coloured bars represent the relative abundance of each species (left y axis), while the white line represents total abundance in cfu/mL (right y axis). Each panel represents average composition across six replicates for each treatment over time. PA14 = *P. aeruginosa*, SA = *S. aureus*, AB = *A. baumannii*, BC = *B.*

cenocepacia, MC = Microbial community. For individual replicates of species abundance, see Fig. S5.

Interestingly, the PA14 WT generally reached greater relative abundance than the CRISPR-KO strain when in the presence of *A. baumannii*, consistently doing so early in the experiment when phage remained in the population (Figs 3 and S2). This was in concordance with *P. aeruginosa* evolving higher levels of CRISPR-based immunity against phage DMS3vir in treatments including *A. baumannii* due to the increased fitness cost of surface modification (Fig S7 and [15]): At 3 days post infection, there was a significant effect of all treatments on the proportion of CRISPR-based resistance that had evolved compared to the PA14 monoculture, but this effect was strongest for treatments that contained *A. baumannii*. At timepoint 10 we only found an increased proportion of *P. aeruginosa* clones immune through CRISPR-Cas when the treatment included *A. baumannii* (GLM; *A. baumannii*; t = 2.637, p = 0.01; *S. aureus* and *A. baumannii*, t = 2.283, p = 0.025; A. *baumannii* and *B. cenocepacia*, t = 2.689, p = 0.0087; polyculture, t = 2.141, p = 0.035).

The type of evolved phage resistance does not have a knock-on effect on microbial community dynamics

We have previously sown that the evolution of phage resistance by mutation of the Type IV pilus (the phage receptor) is associated with large fitness trade-offs in a microbial community context, whereas evolution of CRISPR-based immunity is not associated with any detectable trade-offs [15]. We therefore predicted that the ability to evolve phage

resistance through CRISPR-Cas would also have knock-on effects for the microbial community dynamics. However, measurement of the abundance of the competitors revealed that these were overall largely unaffected by the presence of a functional CRISPR-Cas immune system in *P. aeruginosa* with the exception of *S. aureus*: In the presence of the *P. aeruginosa* WT strain, *S. aureus* densities were significantly lower in two of the microbial communities compared to the same co-culture experiments with the CRISPR-KO strain (Figs 3 and S5, Effect of *P. aeruginosa* clone on *S. aureus* abundance, linear model: Treatment *S. aureus*; t = -2.363, p = 0.0216, adjusted R^2 = 0.2659, $F_{14,57}$= 2.837, p = 0.002786; Treatment *S. aureus* and *A. baumannii*; t = -2.043, p = 0.0457, adjusted R^2 = 0.3867, $F_{14,57}$= 4.198, p = 5.3 x 10^{-5}).

A *P. aeruginosa* targeting phage results in the competitive release of *A. baumannii* and general diversity maintenance

We hypothesised that the effect of phage on microbial community structure could largely be explained by the competitive release (increase in absolute abundance, following removal of competitor) of *A. baumannii*, which then takes over to become the dominant species [55]. To assess this, we examined the fold change difference for the final abundance of all three community members in the presence versus absence of phage (Fig 4). Crucially, this revealed a strong increase in *A. baumannii* density in the presence of a phage, supporting the idea that it becomes the dominant and determinant community member when *P. aeruginosa* is inhibited by phage (Fig 3). By contrast, when phage was added, *S. aureus* only experienced a clear fold change increase if it was co-cultured with the CRISPR-KO strain and an additional competitor species. *B. cenocepacia* meanwhile

245 seemed to be the species with the least benefit of phage, but still with a small fold change
246 increase for some treatments (Fig 4).

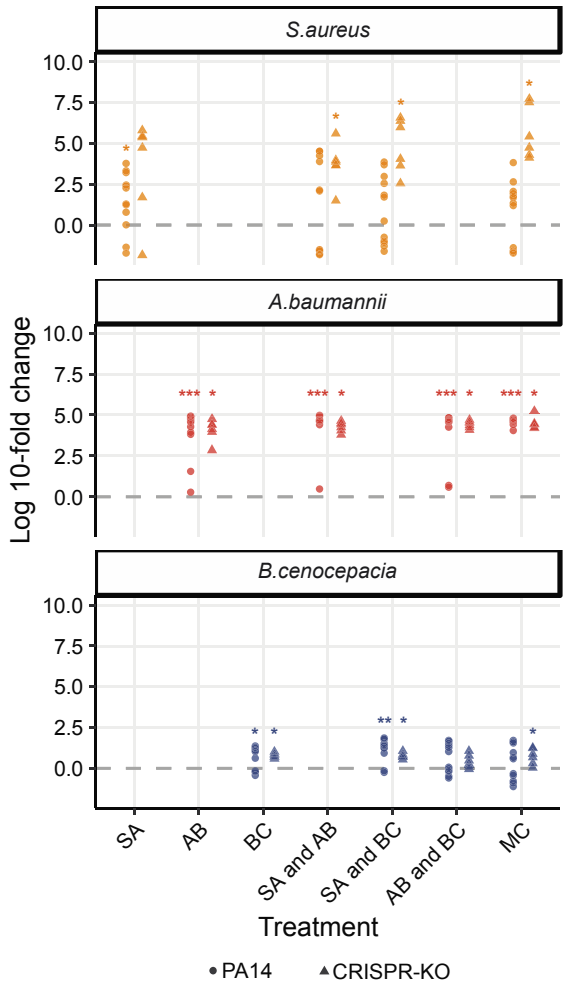

247

248 **Fig 4. Fold change between no phage and phage treatments at the end of the**
249 **experiment.** The fold change difference of the individual community species not targeted
250 by phage when comparing absolute densities in the presence of phage to the absence at
251 the final experimental timepoint. Asterisks indicate higher final absolute density in the
252 presence versus absence of phage (Wilcoxon signed rank exact test: * $p < 0.05$, ** $p <$
253 0.01, *** $p < 0.001$).

254

The substantial 5-fold increase in *A. baumannii* given the presence of phage (Fig 4) reflects a sustained divergence in the trajectory of *A. baumannii* in the phage treatments, despite the attenuation of phage titre by day 7 (Fig S4). We hypothesised that the lack of *P. aeruginosa* rebound after phage clearance was due to a frequency-dependent shift in competitive dominance. To test this hypothesis, we competed ancestral *A. baumannii*, *S. aureus* and *B. cenocepacia* against increasingly rare *P. aeruginosa* challenge, and found no barrier to *P. aeruginosa* invasion in pairwise experiments, down to a frequency of 1 in 10,000 cells (Fig 5). This result suggests that the failure of *P. aeruginosa* to return to dominance following phage clearance is due to more complex community-mediated interactions.

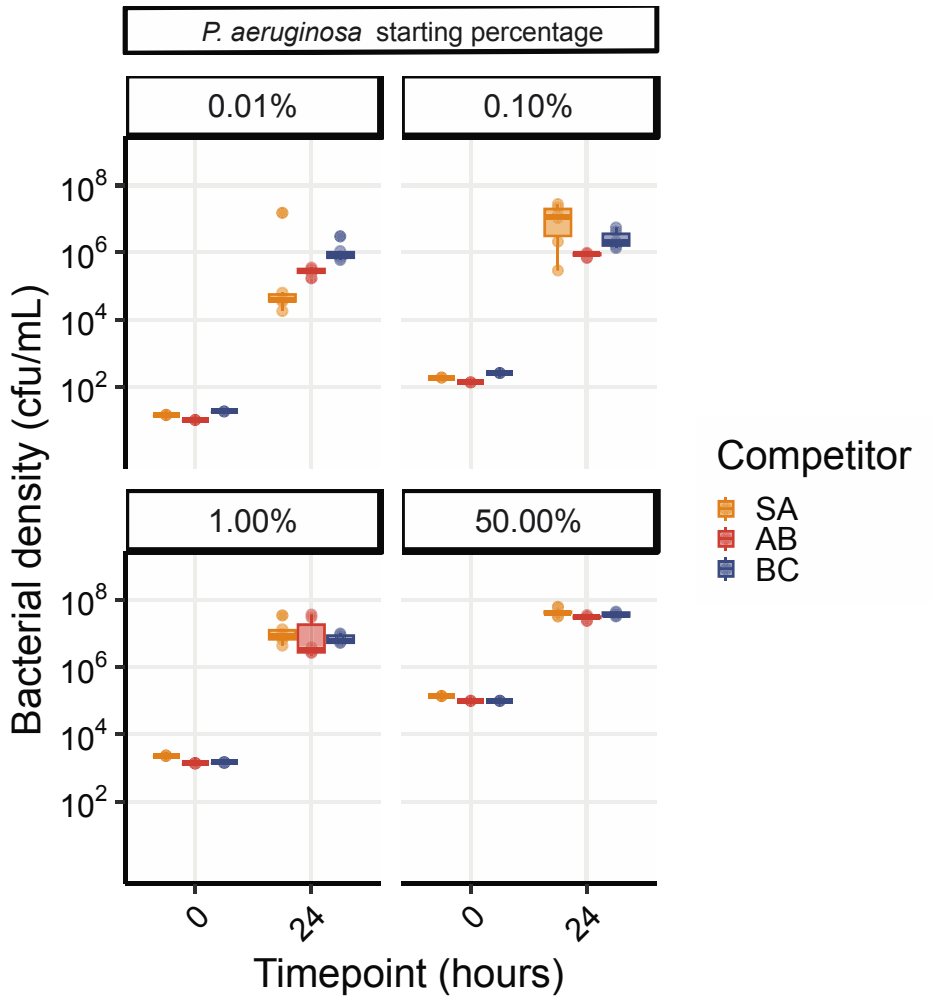

Fig 5. *P. aeruginosa* can reinvade from rare against all community members.

Showing *P. aeruginosa* density in cfu/mL from competition experiments between PA14 wild-type with variable starting densities against either *S. aureus* (SA), *A. baumannii* (AB) or *B. cenocepacia* (BC)**.** The species densities were estimated by qPCR at time-point 0 and 24 h post co-culture. Box plots show the median, 25th and 75th percentile, and the interquartile range. Raw values from each replicate are shown as points (n= 6 per pairwise competition).

To quantitatively assess changes in community diversity, we calculated Shannon diversity indexes for all experimental treatments. We hypothesised that the addition of phage not only results in competitive release of one other bacterium (Fig 4), but facilitates general maintenance of microbial diversity. Plotting these diversity scores over time shows that without phage there is a rapid loss of diversity over time, whereas community complexity persists in the presence of phage (Fig 6: ANOVA: PA14 WT effect of phage; $F = 27.57$, $p = 2.3 \times 10^{-7}$; CRISPR-KO effect of phage; $F = 89.19$, $p < 2.2 \times 10^{-16}$; Overall model fit for PA14 WT: adjusted $R^2 = 0.64$, $F_{38,465} = 24.87$, $p < 2.2 \times 10^{-16}$; Overall model fit for CRISPR-KO: adjusted $R^2 = 0.56$, $F_{32,303} = 14.56$, $p < 2.2 \times 10^{-16}$). This was true for treatments for both *P. aeruginosa* genotypes, but the trend became most pronounced for the CRISPR-KO strain when applying direct comparisons using Tukey contrasts, in which case we found phage to significantly increase diversity over time in nearly all treatments (Fig 6, indicated by asterisks).

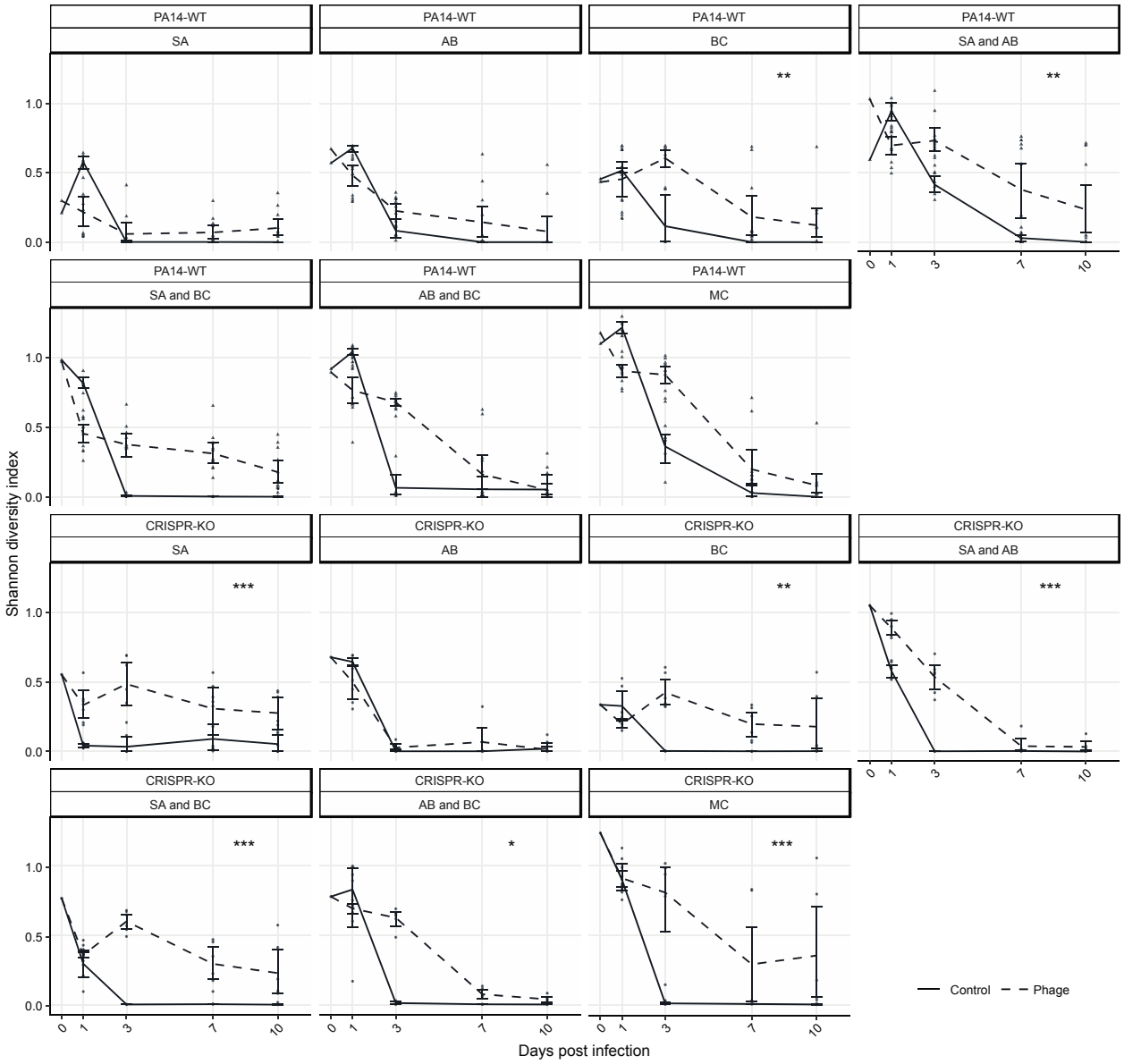

Fig 6. Shannon diversity over time illustrating the diversity maintaining effects of phage. The change in diversity over time, illustrated using Shannon diversity indexes, for both the PA14 WT and CRISPR-KO strains across all treatments (SA = *S. aureus*, AB = *A. baumannii*, BC = *B. cenocepacia,* MC = microbial community). Data are mean ± 95% CI, and asterisks indicate a significant difference over time in Shannon diversity between treatments with phage or no phage (n = 6 per timepoint for all expect the PA14 WT with

295 phage treatments, where n = 12) (effect of *P. aeruginosa* clone; linear model with Tukey
296 contrasts: * $p < 0.05$, ** $p < 0.01$, *** $p < 0.001$).
297

298 Four species community dynamics are predictable from two
299 and three species community data, in the absence of phage

300 A major challenge in synthetic community research is developing robust modelling
301 frameworks that are capable of predicting community dynamics [56]. In a final set of
302 analyses, we sought to assess the predictive performance of generalized Lotka Volterra
303 (gLV) competition equations, trained on just 2-species data or a combination of 2- and 3-
304 species data. Our results showed that fitting gLV models with pairwise only datasets led
305 to predictive failures when applied to 3- or 4-species datasets (Fig S8), consistent with
306 the presence of higher order interactions effects (when the effect of species A on species
307 B is dependent on the presence of species C [57]). In contrast, fitting gLV models to 2-
308 and 3-species data and using the resulting interaction terms to predict 4-species
309 dynamics reasonably fit the data in the absence of phage (Fig 7).
310

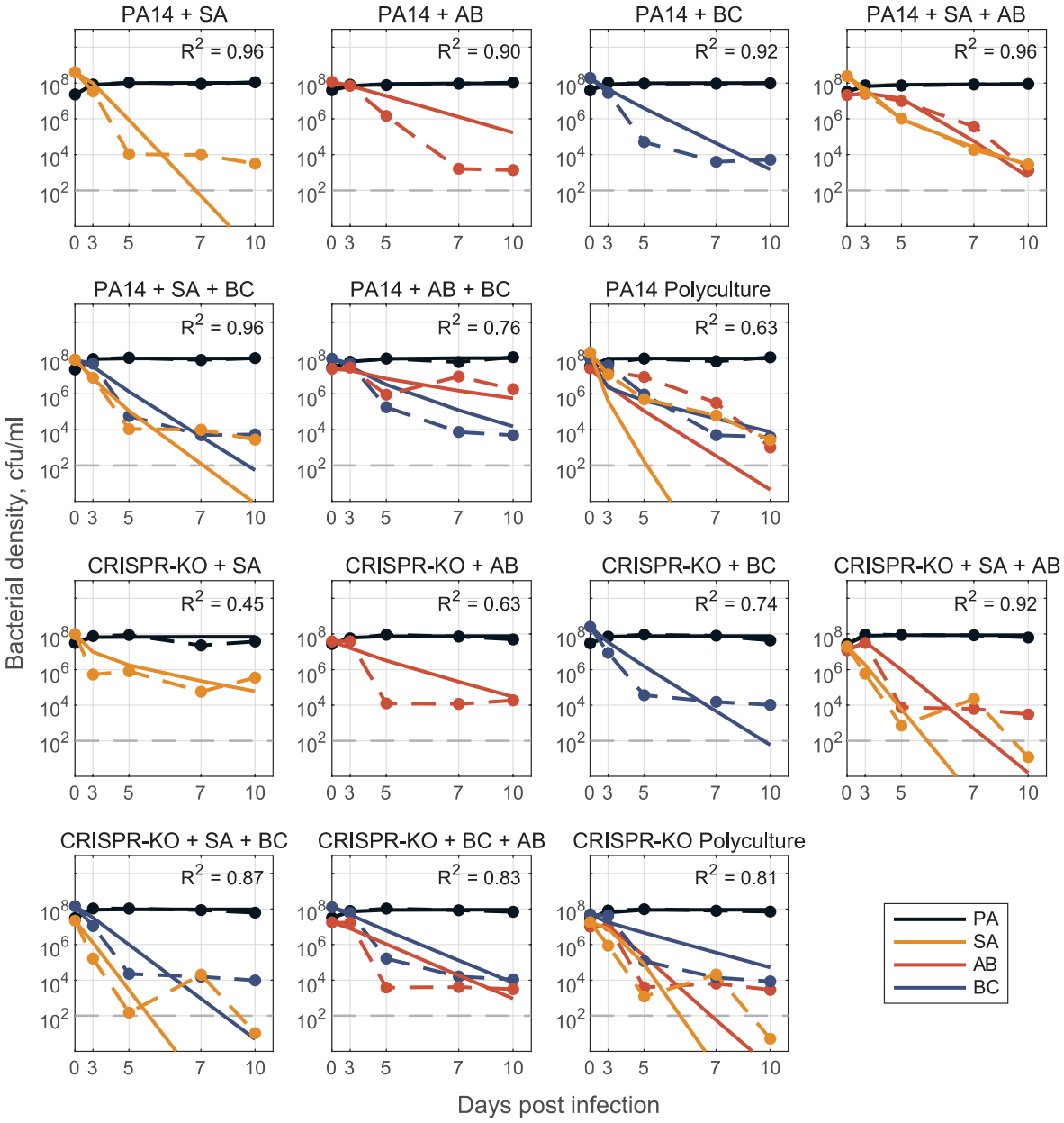

Fig 7. Model for no phage data. Model fit predictions for two-, three-, and full four species community dynamics (solid lines) compared to experimental data (dashed lines). Models of 2- and 3- species dynamics were parameterized via optimization with least-squares to fit to a system of ODEs (defined as a generalized Lotka-Volterra competition model with n species, where n=1,2,3,4). Only single species maximal growth rates (r_i for species $i = 1,..., n$) were fixed from fitting mono-culture data, all

interaction coefficients ($\beta_{i,j}$ describing the inhibitory effect of species j on species i for all $i,j = 1,2$ in the 2-species case, for all $i,j = 1,2,3$ in the 3-species case) were open for fitting. We construct the full 4-species community interaction matrices (one for PA14 and one for CRISPR-KO) by averaging corresponding $\beta_{i,j}$ interaction terms from the fit 2- and 3- species models (see Text S1), and use this matrix to simulate dynamics in the respective polyculture cases. See Methods and Text S1 for detailed description of mathematical modelling.

In the presence of phage (Fig 8), we again utilised the gLV framework where the impact of phage is implicit (quantified by how interaction coefficients change as compared to the no-phage case). The gLV model framework could adequately describe 2- and 3-species data, but the interaction coefficients did not generalise quantitatively to 4-species data – likely reflecting the structural limitation of a gLV competition model that does not explicitly capture phage predation dynamics. However, the model parameterised with 1-, 2- and 3-species data did capture a qualitative shift in ecological outcomes from sole *P. aeruginosa* survival to competitive release of *A. baumannii* and *S. aureus* when *P. aeruginosa* is targeted by phage (Fig S9).

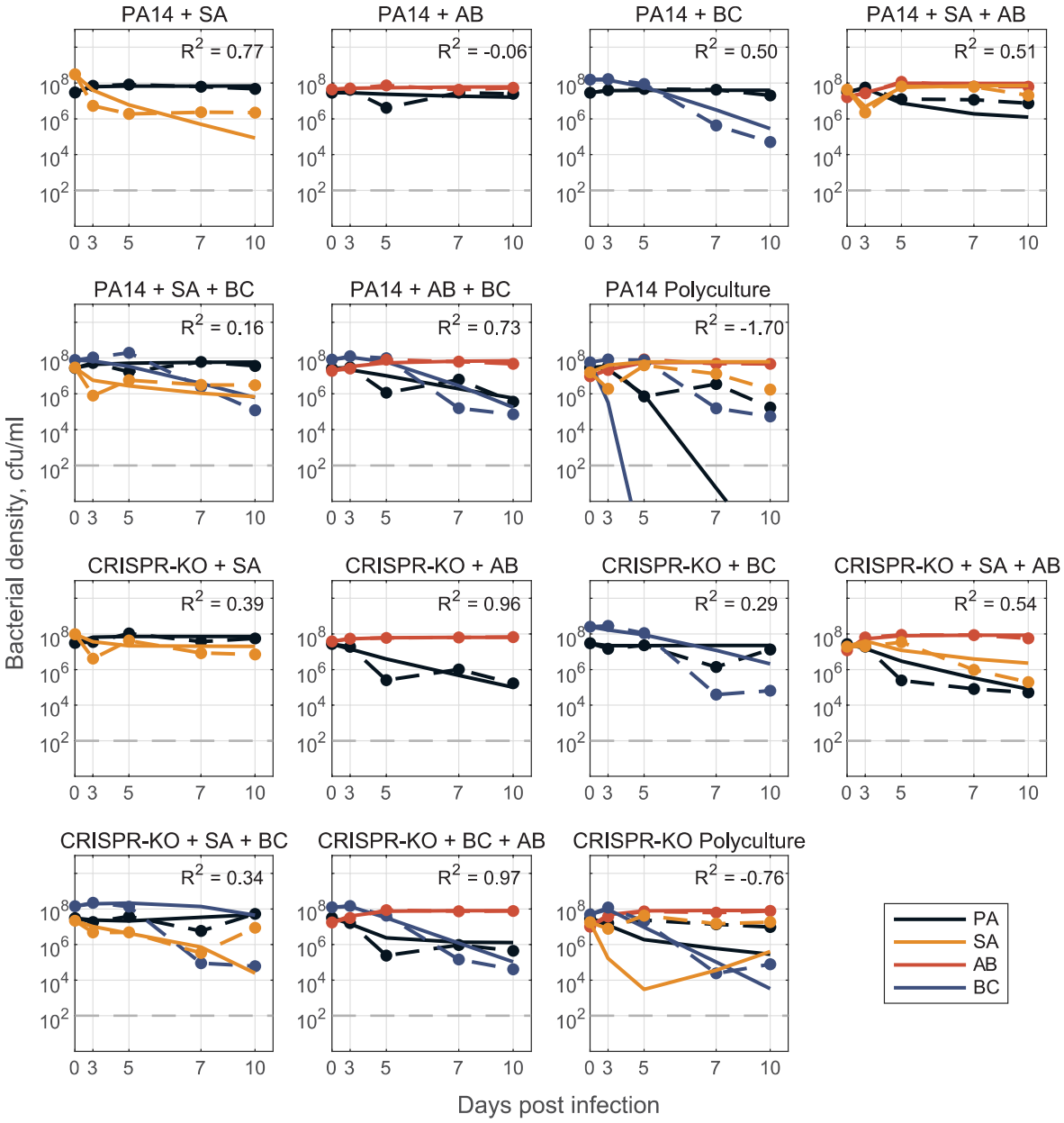

Fig 8. Model for phage data. Model fit predictions for two-, three-, and full four species community dynamics (solid lines) in the presence of phage compared to experimental data (dashed lines). Here, models were parameterized via optimization with least-squares to fit a system of ODEs (defined as a generalized Lotka-Volterra competition model with n species, where n=1,2,3,4), where we don't explicitly track the phage population dynamics. Instead, we assume that the phage acts as some external

perturbation that leads to changes in the interactions between community members ($\beta_{i,j}$ values differ from values in Figure 7). Only single species maximal growth rates were fixed from fitting mono-culture data (r_i for species $i = 1,..., n$), all interaction coefficients were open for parameterizing 2- and 3- species models ($\beta_{i,j}$ describing the inhibitory effect of species j on species i for all $i,j = 1,2$ for the 2-species case, for all $i,j = 1,2,3$ for the 3-species case). We then construct the full 4-species community interaction matrices (one for PA14 and one for CRISPR-KO) by averaging corresponding $\beta_{i,j}$ interaction terms from the fit 3- species models (treatments: PA+AB+SA, PA+BC+SA, PA+AB+BC with phage), and use this matrix to simulate dynamics in the respective polyculture cases. See Methods and Text S1 for detailed description of mathematical modelling.

Discussion

The advent of deep sequencing has dramatically increased our knowledge of the composition and functioning of microbiomes both in and around us. The role of microbial communities in human health has consequentially received increasing attention, with research focusing on how changes in microbiome composition over time may affect human health and define patient outcomes (reviewed in 57). In addition, an increasing number of correlational studies find associations between virome composition and the health status of their host [23,59–61], likely mediated by changes in the microbiome that could be either cause or effect. A deeper understanding of the impact of phages on microbiomes is likely to help to infer causal relationships between viromes and human health, and to design optimal therapeutic phage interventions (phage therapy).

Here, we expanded on our previous work on how interspecific competition can shape the evolution of phage resistance in a focal species (*P. aeruginosa*)[15], to study how the interaction between phage and bacterial immune mechanisms affects the broader microbial community dynamics. We found that whereas *P. aeruginosa* dominated in the absence of a phage, the presence of phage resulted in microbial diversity maintenance and *A. baumannii* becoming the dominant species (Figs 3 and 4). Interestingly, the competitive release of *A. baumannii* occurred in all treatments and was virtually independent of whether *P. aeruginosa* had a functional CRISPR-Cas immune system or not. This showed that the amplification of the fitness cost of *P. aeruginosa* receptor mutation in the presence of competitor species [15] has limited impact on the overall community dynamics. Overall, our experimental data align with the notion of phages having the potential to increase microbiome stability [62,63], and support the idea that phages can be useful in the designing of synthetic microbial communities [64]. Surprisingly, our data do not support the hypothesis that bacterial adaptive immune systems play an important role in phage-mediated microbial community structuring under the experimental conditions tested here.

Our mathematical analyses focused on the ability of generalised Lotka-Volterra (gLV) models to predict community dynamics. While our analyses showed reasonable predictive success when incorporating 3-species data, we note that our analyses pose two distinct questions: (1) how can we provide more accurate predictions? (2) what general lessons can we draw from our model analyses?

In agreement with a growing number of gLV-based analyses, we found that a simple 'bottom up' model fitting approach (fitting single species growth, then all pairwise interactions, then predicting larger system behaviour [14]) performed poorly, indicating the presence of significant higher order interactions [57,65,66]. Consistent with this conclusion, we found that allowing pairwise interactions to vary (contingent on the presence of a third species) produced both qualitative and quantitative improvements in predicting community dynamics (Figs 7 and 8). In the presence of phage, our model successfully predicted the qualitative result of *A. baumannii* competitive release, but failed to quantitatively replicate observed community dynamics (Fig 8). This quantitative failure suggests that our underlying gLV model structure excludes critical components, such as higher order and/or heterogeneous (in time or space) interactions as well as the explicit predatory effect of phage on *P. aeruginosa* (also likely time and spatially dependent). Additionally, it emphasises an ongoing need in microbiome modelling to evaluate functional forms that can efficiently – with respect to parameter number – and accurately capture the complexities of community dynamics.

Our parameterised models are tuned to the data generated by our specific 4-species community, which raises the question of 'can we learn more general lessons from our model?' If we simplify our analysis to a 2-species context (focal pathogen, subject to phage, plus a second, non-focal species), we can translate recent analyses on the impact of (antibiotic) perturbations in a two species context [54]. This approach delivers a couple of general messages. First, we can provide a general mathematical definition of

411 'competitive release' mediated by phage predation (see Text S1) highlighting the
412 importance of both demographic and species interaction parameters. Second, we can
413 underline that phage control of a focal pathogen presents secondary ecological problems,
414 if the pathogen is competing with other pathogens that are not targeted by the phage. In
415 this scenario, phage therapy (or other 'narrow spectrum' treatment) can lead to
416 competitive release of previously rare pathogens, as seen in our experimental data
417 showing the replacement of *P. aeruginosa* by *A. baumannii*, following phage treatment.
418 These results imply that 'narrow spectrum' anti-microbials, such as phages, may not
419 always be the best option when multiple pathogen species are competing within a single
420 polymicrobial infection. One counter-intuitive suggestion, grounded in the idea of
421 'beneficial resistance' [54], is to co-administer probiotic competitors that are resistant to
422 the treatment (i.e. phage or antibiotic resistant) and can therefore continue to exert
423 ecological suppression on the focal pathogen during the course of treatment, while
424 presenting minimal direct risk of disease. Alternatively, one could apply phage cocktails
425 that target not just the dominant pathogen, but also other co-existing bacterial pathogens,
426 to pre-emptively prevent their invasion [67].
427

428 Materials and Methods

429 Bacteria and phages

430 The bacteria *P. aeruginosa* UCBPP-PA14 strain marked with streptomycin resistance,
431 the PA14 *csy3::LacZ* strain (CRISPR-KO), and phages DMS3vir and DMS3vir+acrF1
432 were used throughout this study and have all been previously described [67,68]. The
433 microbial community consisted of *S. aureus* strain 13 S44 S9, *A. baumannii* clinical isolate

FZ21, and *B. cenocepacia* J2315, and were all isolated at Queen Astrid Military Hospital, Brussels, Belgium.

Evolution experiment

The evolution experiment was performed by inoculating 60 µl from overnight cultures, that were grown for 24 hours, into glass microcosms containing 6 ml fresh LB medium (60 µl of culture containing ca. 10^6 cfu). All polyculture mixes were prepared so that *P. aeruginosa* made up approximately 25% of the total inoculation volume (15 µl of 60 µl), with the rest being made up of one or equal amounts of the microbial community bacteria. In all monoculture controls, *P. aeruginosa* was diluted in LB medium to adjust starting densities for consistency across all treatments (n = 6 per treatment, unless indicated otherwise). Phage DMS3vir was added at 10^6 PFU. prior to inoculation. The experiment ran for ten days, with transfers of 1:100 into fresh LB medium being done every 24 hours. Throughout the experiment, the bacterial mixtures were grown at 37°C and shaking at 180 r.p.m. Phage titres were monitored daily, and were determined using chloroform-treated lysate dilutions which were spotted onto lawns of *P. aeruginosa csy::LacZ*. To determine which mechanism of phage-resistance had evolved, 24 randomly selected clones per treatment replica from timepoints 3 and 10 were analysed using methods as detailed in Westra *et al*. 2015 [68].

DNA extraction and qPCR

Bacterial densities, for both PA14 strains and the other individual microbial community bacteria, were determined using DNA extractions followed by qPCR analyses. DNA

457 extractions were done using the DNeasy UltraClean Microbial Kit (Qiagen), following
458 instructions from the manufacturer, but with an additional pre-extraction step where
459 samples were treated with 15 µl lysostaphin (Sigma) at 0.1 mg ml^{-1} as previously
460 described [15] to ensure lysis of *S. aureus*. The qPCR primers for *P. aeruginosa*, *A.*
461 *baumannii*, and *B. cenocepacia* were the same as in Alseth *et al*. [15], whereas the *S.*
462 *aureus* primers used are previously described [69]. All reactions were done in triplicates,
463 using Brilliant SYBR Green reagents (Agilent) and the Applied Biosystems QuantStudio
464 7 Flex Real-Time PCR system. For reaction mixture and details on PCR programme, see
465 ref. [15]. Bacterial cfu/ mL were calculated from the quantities offered by the standard
466 curve method, adjusting for gene copy number (4, 1, 6, and 6, for *P. aeruginosa*, *S.*
467 *aureus*, *A. baumannii*, and *B. cenocepacia* respectively).
468

469 ## Competition experiment

470 All strains were grown overnight at 37ºC with agitation in 30 ml glass universals containing
471 6 ml of LB medium. For pairwise competition assays, bacteria from overnight cultures
472 were mixed thoroughly at different starting densities of PA14 (i.e., for 50% starting density
473 o *P. aeruginosa* - 30 µl of PA14 + 30 µl of competitor strain) and a total of 60 µl inoculated
474 into 6 ml of LB (*n* = 6 per treatment). Bacteria were grown for 24 hours in a shaking
475 incubator at 180 r.p.m at 37ºC. Samples of 500 µl were taken at 0 and 24 hours post
476 competition and mixed with equal volume of 60% glycerol and stored at -70ºC until further
477 DNA extraction and qPCR analysis to quantify species densities.
478

To determine the competitive performance of the focal species relative to competitor strain we used the selection rate (r) formula as it follows: (r) each day (t) 1 (n) day post incubation (r = (ln [density strain A at t_n/density strain A at t_{n-1}] – ln [density strain B at t_n/density strain B at t_{n-1}])/day) [70,71].

Mathematical modelling

Models were parameterized via optimization with least-squares regression to fit the generalized Lotka-Volterra competition model, $\frac{dN_i}{dt} = r_i N_i - \sum_{j=1}^{n} \beta_{ij} N_i N_j$, where $N_i(t)$ is the density of the ith species, r_i is the respective single species maximal growth rate, β_{ij} describes the per capita effect of species j on species i, and n is the total number of species. We take a 'bottom up' approach [72] to determine the interaction coefficients $\beta_{i,j}$. In all cases, we determine single species maximal growth rates r_i from mono-culture time series data and fix them for 2-, 3-, and 4-species model parameterization. Initially, we fit pairwise interaction coefficients for all possible 2-species co-cultures and from here, construct an interaction matrix to predict the dynamics for the 3- and 4- species communities (Fig S8). This is done for both PA14 and CRISPR-KO strains, with and without phage, where phage effects are implicitly represented by changes in interaction parameters between the models with and without phage. To improve results, we additionally fit pairwise interaction parameters $\beta_{i,j}$ using 3-species experimental data where all interaction parameters are open (only growth rates fixed). Using either the resulting interaction terms or averaging these coefficients with the 2-species coefficients (in PA14 no phage case, Text S1), we are again able to construct an interaction matrix to predict 4-species community dynamics (Fig 7 and 8).

See Text S1 for further description of above model parameterization methods, simulation methods (Fig S9), and mathematical analysis of phage dependent competitive release. All modelling and analysis was done using Matlab 2021b and the code is publicly available at: https://github.com/GaTechBrownLab/phage-community-dynamics.git.

Statistical analyses

Analysis of the effects of the various species compositions on *P. aeruginosa* densities in the absence (Fig 2) or presence (Fig 3) of phage were done using a generalised linear model (GLM) approach, with log10 cfu/mL set as the response variable. The explanatory variables used in the analyses were type of PA14 clone (PA14 WT or CRISPR-KO), treatment, timepoint, replica, and experimental repeat to account for potential pseudo-replication.

To explore the impact of interspecific competition on the evolution of phage resistance at timepoints 3 and 10 (Fig S7), we used a quasibinomial GLM where the proportion of evolved CRISPR-based phage resistance was the response variable, and treatment, replica, and experimental repeat were the explanatory variables.

The analyses of fold-changes to assess competitive release by comparing absolute density differences of the individual community members in the absence v presence of phage (Fig 4; *S. aureus*, *A. baumannii*, and *B. cenocepacia*) was done through Wilcox signed rank exact tests. A non-parametric test was chosen after performing a Shapiro-Wilk test for normality.

Next, the diversity maintaining effects were examined through assessing the effect of phage DMS3vir on Shannon Diversity index scores over time (Fig 5). This was done through a linear model where the Shannon Diversity index score (H) was the response variable, and treatment, timepoint, the presence of phage, PA14 clone (PA14WT and CRISPR-KO), experimental repeat, and replica were the explanatory variables. Shannon Diversity (H), was calculated as $H = -\Sigma p_i * \ln(p_i)$, where Σ is the sum and p_i is the proportion of the entire community made up of species *i*.

For the competition assay (Fig 5), Graphpad Prism9 software (San Diego, CA) was used for statistical analysis. We used one-way ANOVA with Tukey post hoc testing for multiple comparisons, in which, $p < 0.05$ was considered statistically significant.

Throughout the paper, pairwise comparisons were done using the Emmeans package [73], and model fits were assessed using Chi-squared tests and by comparing Akaike information criterion (AIC) values, as well as plotting residuals and probability distributions using histograms and quantile-quantile plots (Q-Q plots) respectively. All statistical analyses were done using R version 4.3.0. [74], its built-in methods, and the Tidyverse package version 2.0.0 [75]. All data is available at: 10.6084/m9.figshare.24187284.

Acknowledgements

This work was supported by a grant from the ERC (ERC-STG-2016-714478 - EVOIMMECH), a Biotechnology and Biological Sciences Research Council (BBSRC) sLoLa grant BB/X003051/1, awarded to E.R.W, a NHI grant (NIH 5R21AI156817-02) awarded to S.P.B, and a BBSRC-National Science Foundation (NSF) grant xxxx, awarded to S.P.B., R.A.K & E.R.W.

Competing Interests

E.R.W. is inventor on patent GB2303034.9.

References

1. Byrd AL, Belkaid Y, Segre JA. The human skin microbiome. Nat Rev Microbiol. 2018;16: 143–155. doi:10.1038/nrmicro.2017.157

2. Thursby E, Juge N. Introduction to the human gut microbiota. Biochem J. 2017;474: 1823–1836. doi:10.1042/BCJ20160510

3. Pearl Mizrahi S, Goyal A, Gore J. Community interactions drive the evolution of antibiotic tolerance in bacteria. Proc Natl Acad Sci. 2023;120: e2209043119. doi:10.1073/pnas.2209043119

4. Manichanh C, Borruel N, Casellas F, Guarner F. The gut microbiota in IBD. Nat Rev Gastroenterol Hepatol. 2012;9: 599–608. doi:10.1038/nrgastro.2012.152

5. Freitas AC, Chaban B, Bocking A, Rocco M, Yang S, Hill JE, et al. The vaginal microbiome of pregnant women is less rich and diverse, with lower prevalence of Mollicutes, compared to non-pregnant women. Sci Rep. 2017;7: 9212. doi:10.1038/s41598-017-07790-9

6. Lloyd-Price J, Mahurkar A, Rahnavard G, Crabtree J, Orvis J, Hall AB, et al. Strains, functions and dynamics in the expanded Human Microbiome Project. Nature. 2017;550: 61–66. doi:10.1038/nature23889

7. Glassner KL, Abraham BP, Quigley EMM. The microbiome and inflammatory bowel disease. J Allergy Clin Immunol. 2020;145: 16–27. doi:10.1016/j.jaci.2019.11.003

8. Azimi S, Lewin GR, Whiteley M. The biogeography of infection revisited. Nat Rev Microbiol. 2022;20: 579–592. doi:10.1038/s41579-022-00683-3

9. Scher JU, Sczesnak A, Longman RS, Segata N, Ubeda C, Bielski C, et al. Expansion of intestinal *Prevotella copri* correlates with enhanced susceptibility to arthritis. Mathis D, editor. eLife. 2013;2: e01202. doi:10.7554/eLife.01202

10. Lam V, Su J, Hsu A, Gross GJ, Salzman NH, Baker JE. Intestinal microbial metabolites are linked to severity of myocardial infarction in rats. PloS One. 2016;11: e0160840. doi:10.1371/journal.pone.0160840

11. Livanos AE, Greiner TU, Vangay P, Pathmasiri W, Stewart D, McRitchie S, et al. Antibiotic-mediated gut microbiome perturbation accelerates development of type 1 diabetes in mice. Nat Microbiol. 2016;1: 16140. doi:10.1038/nmicrobiol.2016.140

12. Surana NK, Kasper DL. Moving beyond microbiome-wide associations to causal microbe identification. Nature. 2017;552: 244–247. doi:10.1038/nature25019

13. Castledine M, Padfield D, Buckling A. Experimental (co)evolution in a multi-species microbial community results in local maladaptation. Ecol Lett. 2020;23: 1673–1681. doi:10.1111/ele.13599

14. Varga JJ, Zhao CY, Davis JD, Hao Y, Farrell JM, Gurney JR, et al. Antibiotics drive expansion of rare pathogens in a chronic infection microbiome model. mSphere. 2022;7: e00318-22. doi:10.1128/msphere.00318-22

15. Alseth EO, Pursey E, Luján AM, McLeod I, Rollie C, Westra ER. Bacterial biodiversity drives the evolution of CRISPR-based phage resistance. Nature. 2019;574: 549–552. doi:10.1038/s41586-019-1662-9

16. Piccardi P, Vessman B, Mitri S. Toxicity drives facilitation between 4 bacterial species. Proc Natl Acad Sci. 2019;116: 15979–15984. doi:10.1073/pnas.1906172116

17. Großkopf T, Soyer OS. Synthetic microbial communities. Curr Opin Microbiol. 2014;18: 72–77. doi:10.1016/j.mib.2014.02.002

18. De Roy K, Marzorati M, Van den Abbeele P, Van de Wiele T, Boon N. Synthetic microbial ecosystems: an exciting tool to understand and apply microbial communities: Synthetic microbial ecosystems. Environ Microbiol. 2014;16: 1472–1481. doi:10.1111/1462-2920.12343

19. Karkaria BD, Manhart A, Fedorec AJH, Barnes CP. Chaos in synthetic microbial communities. PLOS Comput Biol. 2022;18: e1010548. doi:10.1371/journal.pcbi.1010548

20. Wang T, Weiss A, Aqeel A, Wu F, Lopatkin AJ, David LA, et al. Horizontal gene transfer enables programmable gene stability in synthetic microbiota. Nat Chem Biol. 2022; 1–8. doi:10.1038/s41589-022-01114-3

606 21. Dion MB, Oechslin F, Moineau S. Phage diversity, genomics and phylogeny. Nat
607 Rev Microbiol. 2020;18: 125–138. doi:10.1038/s41579-019-0311-5

608 22. Suttle CA. Viruses in the sea. Nature. 2005;437: 356–361. doi:10.1038/nature04160

609 23. Chevallereau A, Pons BJ, van Houte S, Westra ER. Interactions between bacterial
610 and phage communities in natural environments. Nat Rev Microbiol. 2021; 1–14.
611 doi:10.1038/s41579-021-00602-y

612 24. Sullivan MB, Weitz JS, Wilhelm S. Viral ecology comes of age. Environ Microbiol
613 Rep. 2017;9: 33–35. doi:https://doi.org/10.1111/1758-2229.12504

614 25. Fazzino L, Anisman J, Chacón JM, Heineman RH, Harcombe WR. Lytic
615 bacteriophage have diverse indirect effects in a synthetic cross-feeding community.
616 ISME J. 2020;14: 123–134. doi:10.1038/s41396-019-0511-z

617 26. Castledine M, Sierocinski P, Inglis M, Kay S, Hayward A, Buckling A, et al. Greater
618 phage genotypic diversity constrains arms-race coevolution. Front Cell Infect
619 Microbiol. 2022;12: 834406. doi:10.3389/fcimb.2022.834406

620 27. Tecon R, Mitri S, Ciccarese D, Or D, van der Meer JR, Johnson DR. Bridging the
621 holistic-reductionist divide in microbial ecology. mSystems. 2019;4: e00265-18,
622 /msystems/4/1/msys.00265-18.atom. doi:10.1128/mSystems.00265-18

623 28. Blazanin M, Turner PE. Community context matters for bacteria-phage ecology and
624 evolution. ISME J. 2021; 1–10. doi:10.1038/s41396-021-01012-x

625 29. Clooney AG, Sutton TDS, Shkoporov AN, Holohan RK, Daly KM, O'Regan O, et al.
626 Whole-virome analysis sheds light on viral dark matter in Inflammatory Bowel
627 Disease. Cell Host Microbe. 2019;26: 764-778.e5. doi:10.1016/j.chom.2019.10.009

628 30. Norman JM, Handley SA, Baldridge MT, Droit L, Liu CY, Keller BC, et al. Disease-
629 specific alterations in the enteric virome in Inflammatory Bowel Disease. Cell.
630 2015;160: 447–460. doi:10.1016/j.cell.2015.01.002

631 31. Zuo T, Lu X-J, Zhang Y, Cheung CP, Lam S, Zhang F, et al. Gut mucosal virome
632 alterations in ulcerative colitis. Gut. 2019;68: 1169–1179. doi:10.1136/gutjnl-2018-
633 318131

634 32. Ma Y, You X, Mai G, Tokuyasu T, Liu C. A human gut phage catalog correlates the
635 gut phageome with type 2 diabetes. Microbiome. 2018;6: 24. doi:10.1186/s40168-
636 018-0410-y

637 33. Tetz G, Brown SM, Hao Y, Tetz V. Parkinson's disease and bacteriophages as its
638 overlooked contributors. Sci Rep. 2018;8: 10812. doi:10.1038/s41598-018-29173-4

639 34. Mirzaei MK, Khan MAA, Ghosh P, Taranu ZE, Taguer M, Ru J, et al. Bacteriophages
640 isolated from stunted children can regulate gut bacterial communities in an age-
641 specific manner. Cell Host Microbe. 2020;27: 199-212.e5.
642 doi:10.1016/j.chom.2020.01.004

643 35. Mayo-Muñoz D, Pinilla-Redondo R, Birkholz N, Fineran PC. A host of armor:
644 Prokaryotic immune strategies against mobile genetic elements. Cell Rep. 2023;42.
645 doi:10.1016/j.celrep.2023.112672

646 36. Georjon H, Bernheim A. The highly diverse antiphage defence systems of bacteria.
647 Nat Rev Microbiol. 2023; 1–15. doi:10.1038/s41579-023-00934-x

648 37. Labrie SJ, Samson JE, Moineau S. Bacteriophage resistance mechanisms. Nat Rev
649 Microbiol. 2010;8: 317–327. doi:10.1038/nrmicro2315

650 38. Bikard D, Marraffini LA. Innate and adaptive immunity in bacteria: mechanisms of
651 programmed genetic variation to fight bacteriophages. Curr Opin Immunol. 2012;24:
652 15–20. doi:10.1016/j.coi.2011.10.005

653 39. Rostøl JT, Marraffini L. (Ph)ighting Phages: How Bacteria Resist Their Parasites.
654 Cell Host Microbe. 2019;25: 184–194. doi:10.1016/j.chom.2019.01.009

655 40. Dimitriu T, Szczelkun MD, Westra ER. Evolutionary ecology and interplay of
656 prokaryotic innate and adaptive immune systems. Curr Biol CB. 2020;30: R1189–
657 R1202. doi:10.1016/j.cub.2020.08.028

658 41. Harvey H, Bondy-Denomy J, Marquis H, Sztanko KM, Davidson AR, Burrows LL.
659 *Pseudomonas aeruginosa* defends against phages through type IV pilus
660 glycosylation. Nat Microbiol. 2018;3: 47–52. doi:10.1038/s41564-017-0061-y

661 42. Barrangou R, Fremaux C, Deveau H, Richards M, Boyaval P, Moineau S, et al.
662 CRISPR provides acquired resistance against viruses in prokaryotes. Science.
663 2007;315: 1709–1712. doi:10.1126/science.1138140

664 43. Laanto E, Bamford JKH, Laakso J, Sundberg L-R. Phage-driven loss of virulence in
665 a fish pathogenic bacterium. PLoS ONE. 2012;7: e53157.
666 doi:10.1371/journal.pone.0053157

667 44. León M, Bastías R. Virulence reduction in bacteriophage resistant bacteria. Front
668 Microbiol. 2015;6. doi:10.3389/fmicb.2015.00343

669 45. Hosseinidoust Z, Tufenkji N, van de Ven TGM. Formation of biofilms under phage
670 predation: considerations concerning a biofilm increase. Biofouling. 2013;29: 457–
671 468. doi:10.1080/08927014.2013.779370

672 46. Chan BK, Sistrom M, Wertz JE, Kortright KE, Narayan D, Turner PE. Phage selection
673 restores antibiotic sensitivity in MDR *Pseudomonas aeruginosa*. Sci Rep. 2016;6:
674 26717. doi:10.1038/srep26717

675 47. Bhargava N, Sharma P, Capalash N. Pyocyanin stimulates quorum sensing-
676 mediated tolerance to oxidative stress and increases persister cell populations in
677 *Acinetobacter baumannii*. Infect Immun. 2014;82: 3417–3425.
678 doi:10.1128/IAI.01600-14

679 48. Drevinek P, Mahenthiralingam E. *Burkholderia cenocepacia* in cystic fibrosis:
680 epidemiology and molecular mechanisms of virulence. Clin Microbiol Infect. 2010;16:
681 821–830. doi:10.1111/j.1469-0691.2010.03237.x

682 49. Pendleton JN, Gorman SP, Gilmore BF. Clinical relevance of the ESKAPE
683 pathogens. Expert Rev Anti Infect Ther. 2013;11: 297–308. doi:10.1586/eri.13.12

684 50. Stacy A, McNally L, Darch SE, Brown SP, Whiteley M. The biogeography of
685 polymicrobial infection. Nat Rev Microbiol. 2016;14: 93–105.
686 doi:10.1038/nrmicro.2015.8

687 51. Thingstad TF. Elements of a theory for the mechanisms controlling abundance,
688 diversity, and biogeochemical role of lytic bacterial viruses in aquatic systems.
689 Limnol Oceanogr. 2000;45: 1320–1328. doi:10.4319/lo.2000.45.6.1320

690 52. de Roode JC, Culleton R, Bell AS, Read AF. Competitive release of drug resistance
691 following drug treatment of mixed *Plasmodium chabaudi* infections. Malar J. 2004;3:
692 33. doi:10.1186/1475-2875-3-33

693 53. Wale N, Sim DG, Jones MJ, Salathe R, Day T, Read AF. Resource limitation
694 prevents the emergence of drug resistance by intensifying within-host competition.
695 Proc Natl Acad Sci. 2017;114: 13774–13779. doi:10.1073/pnas.1715874115

696 54. Wollein Waldetoft K, Sundius S, Kuske R, Brown SP. Defining the benefits of
697 antibiotic resistance in commensals and the scope for resistance optimization. mBio.
698 2022;14: e01349-22. doi:10.1128/mbio.01349-22

699 55. Lloyd-Smith JO. Vacated niches, competitive release and the community ecology of
700 pathogen eradication. Philos Trans R Soc B Biol Sci. 2013;368: 20120150.
701 doi:10.1098/rstb.2012.0150

702 56. Widder S, Allen RJ, Pfeiffer T, Curtis TP, Wiuf C, Sloan WT, et al. Challenges in
703 microbial ecology: building predictive understanding of community function and
704 dynamics. ISME J. 2016;10: 2557–2568. doi:10.1038/ismej.2016.45

705 57. Wootton JT. The nature and consequences of indirect effects in ecological
706 communities. 1994. doi:10/dzfmpb

707 58. Petersen C, Round JL. Defining dysbiosis and its influence on host immunity and
708 disease. Cell Microbiol. 2014;16: 1024–1033. doi:10.1111/cmi.12308

709 59. Waller AS, Yamada T, Kristensen DM, Kultima JR, Sunagawa S, Koonin EV, et al.
710 Classification and quantification of bacteriophage taxa in human gut metagenomes.
711 ISME J. 2014;8: 1391–1402. doi:10.1038/ismej.2014.30

712 60. Dahlman S, Avellaneda-Franco L, Barr JJ. Phages to shape the gut microbiota? Curr
713 Opin Biotechnol. 2021;68: 89–95. doi:10.1016/j.copbio.2020.09.016

714 61. Sweere JM, Van Belleghem JD, Ishak H, Bach MS, Popescu M, Sunkari V, et al.
715 Bacteriophage trigger antiviral immunity and prevent clearance of bacterial infection.
716 Science. 2019;363: eaat9691. doi:10.1126/science.aat9691

717 62. Coyte KZ, Schluter J, Foster KR. The ecology of the microbiome: Networks,
718 competition, and stability. Science. 2015;350: 663–666.
719 doi:10.1126/science.aad2602

720 63. Hofbauer J, Sigmund K. On the stabilizing effect of predators and competitors on
721 ecological communities. J Math Biol. 1989;27: 537–548. doi:10.1007/BF00288433

722 64. Coyte KZ, Rao C, Rakoff-Nahoum S, Foster KR. Ecological rules for the assembly
723 of microbiome communities. PLoS Biol. 2021;19: e3001116.
724 doi:10.1371/journal.pbio.3001116

65. Bairey E, Kelsic ED, Kishony R. High-order species interactions shape ecosystem diversity. Nat Commun. 2016;7: 12285. doi:10.1038/ncomms12285

66. Grilli J, Barabás G, Michalska-Smith MJ, Allesina S. Higher-order interactions stabilize dynamics in competitive network models. Nature. 2017;548: 210–213. doi:10.1038/nature23273

67. van Houte S, Ekroth AKE, Broniewski JM, Chabas H, Ashby B, Bondy-Denomy J, et al. The diversity-generating benefits of a prokaryotic adaptive immune system. Nature. 2016;532: 385–388. doi:10.1038/nature17436

68. Westra ER, van Houte S, Oyesiku-Blakemore S, Makin B, Broniewski JM, Best A, et al. Parasite exposure drives selective evolution of constitutive versus inducible defense. Curr Biol. 2015;25: 1043–1049. doi:10.1016/j.cub.2015.01.065

69. Goto M, Takahashi H, Segawa Y, Hayashidani H, Takatori K, Hara-Kudo Y. Real-time PCR method for quantification of *Staphylococcus aureus* in milk. J Food Prot. 2007;70: 90–96. doi:10.4315/0362-028X-70.1.90

70. Lenski RE, Rose MR, Simpson SC, Tadler SC. Long-term experimental evolution in *Escherichia coli*. I. Adaptation and divergence during 2,000 generations. Am Nat. 1991;138: 1315–1341. doi:10.1086/285289

71. Travisano M, Lenski RE. Long-Term Experimental evolution in *Escherichia coli*. IV. Targets of selection and the specificity of adaptation. Genetics. 1996;143: 15–26. doi:10.1093/genetics/143.1.15

745 73. Davis JD, Olivença DV, Brown SP, Voit EO. Methods of quantifying interactions
746 among populations using Lotka-Volterra models. Front. Syst. Biol. 2022;2.
747 doi.org/10.3389/fsysb.2022.1021897

748 73. Lenth RV. Least-squares means: The R package lsmeans. J Stat Softw. 2016;69:
749 1–33. doi:10.18637/jss.v069.i01

750 74. R Core Team. R: A language and environment for statistical computing. R
751 Foundation for Statistical Computing, Vienna, Austria. 2020. Available:
752 https://www.R-project.org/

753 75. Wickham H, Averick M, Bryan J, Chang W, McGowan LD, François R, et al.
754 Welcome to the Tidyverse. J Open Source Softw. 2019;4. doi:10.21105/joss.01686

755

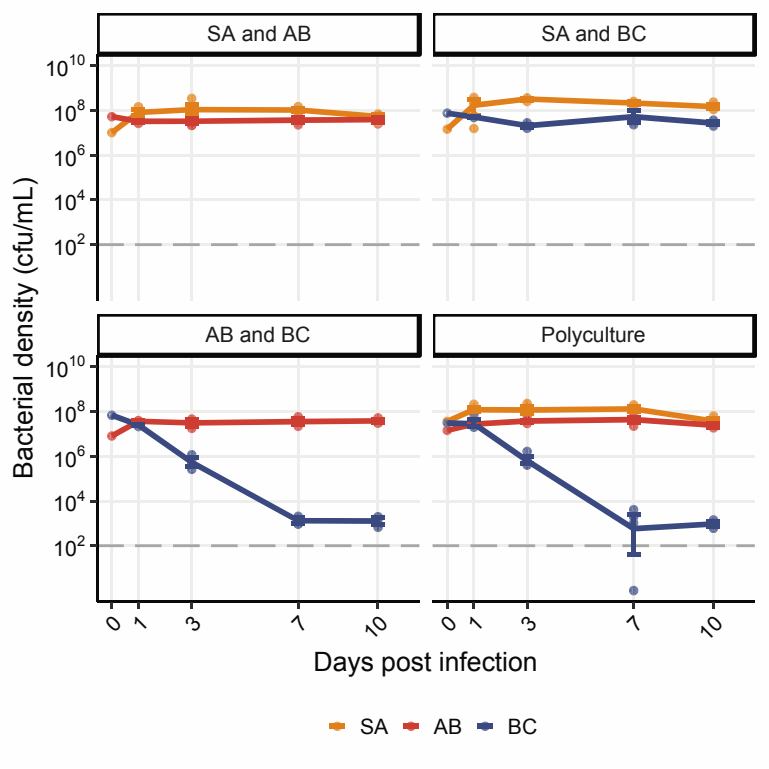

Supplemental Fig 1. Line plot of bacterial densities in the absence of *P. aeruginosa* and its phage. Showing the bacterial densities in cfu/mL over time for SA (*S. aureus*), AB (*A. baumannii*), and BC (*B. cenocepacia*) in various co-culture combinations in the absence of *P. aeruginosa* and its phage. Dashed horizontal line at 10^2 cfu/mL marks the threshold of reliable detection where the qPCR results indicate the bacteria has gone or is close to extinction from a population. Data are mean ± 95% CI.

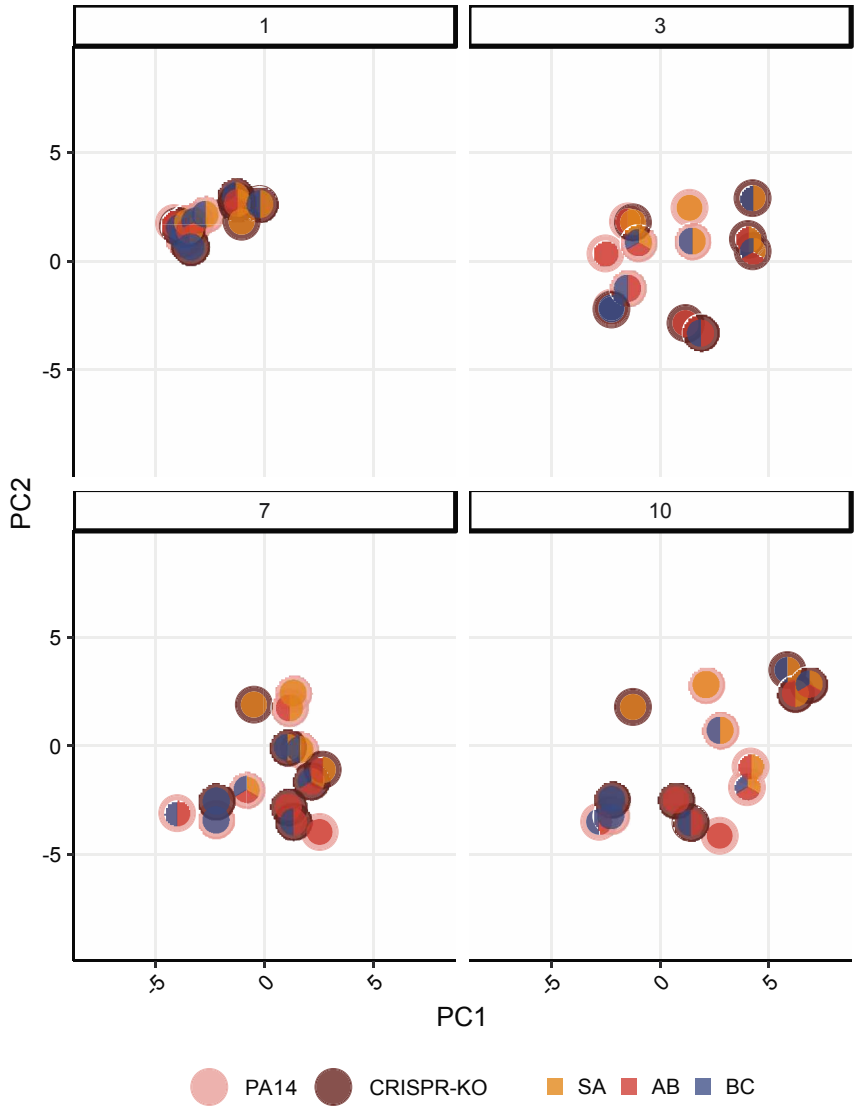

764

765 **Supplemental Fig 2. Ordination plot in the absence of phage.** PCA ordination of
766 relative bacterial abundance in the absence of phage DMS3vir, with grid layouts
767 separated into days post phage infection. Outer circle colour indicates which PA14 clone
768 is present in the population, while inner circle indicates community composition (SA = *S.*
769 *aureus*, AB = *A. baumannii*, BC = *B. cenocepacia*).

770

771

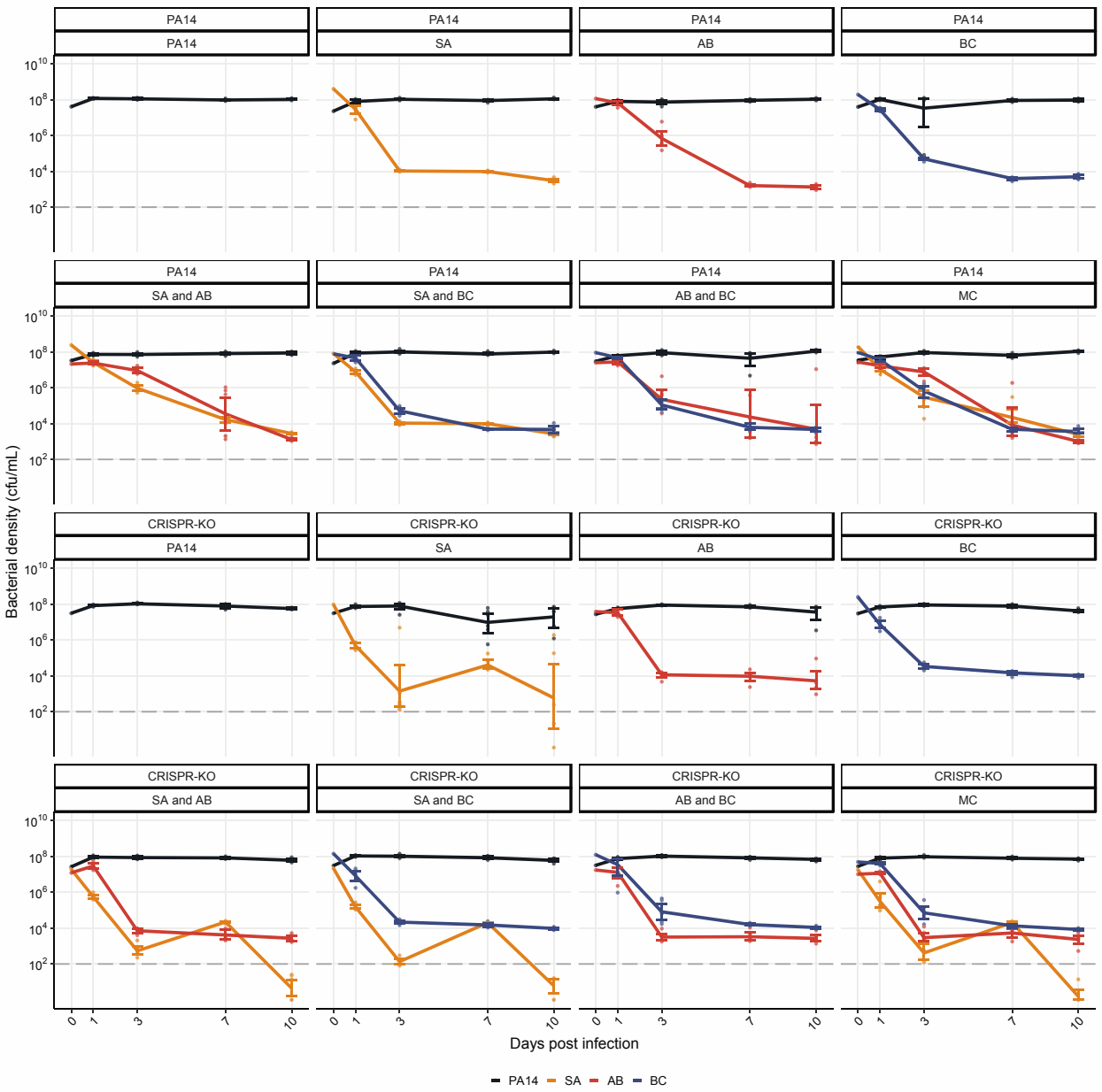

Supplemental Fig 3. Line plots of bacterial densities in the absence of phage. Showing the bacterial densities in cfu/mL over time for the PA14 WT and CRISPR-KO *P. aeruginosa* strains, and **b** the other microbial community species (SA = *S. aureus*, AB = *A. baumannii*, BC = *B. cenocepacia,* MC = microbial community) in the absence of phage DMS3vir. Dashed horizontal line at 10^2 cfu/mL marks the threshold of reliable detection

778 where the qPCR results indicate the bacteria has gone or is close to extinction from a

779 population. Data are mean ± 95% CI.

780

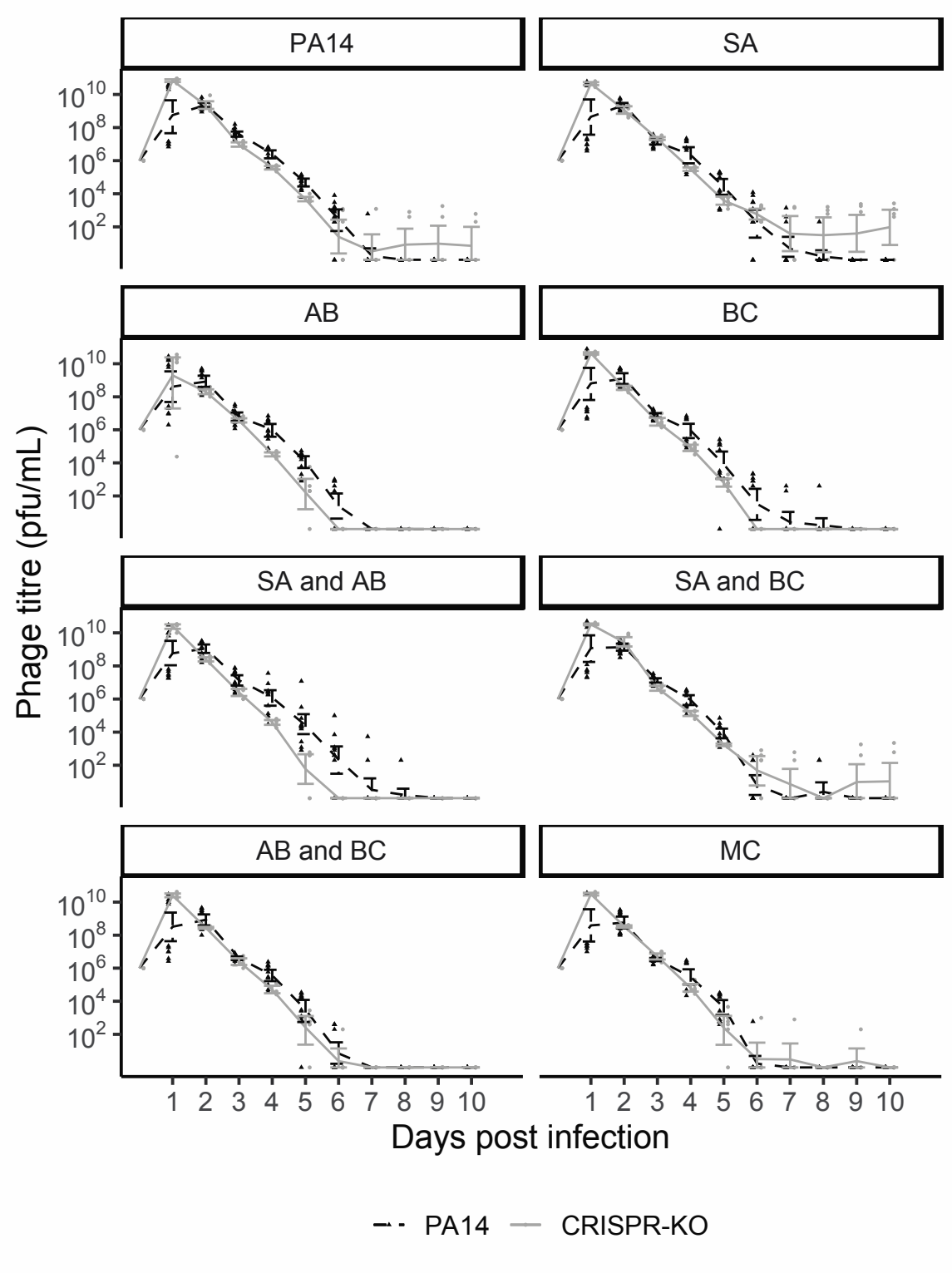

781

782 **Supplemental Fig 4. Phage titres over time for each experimental treatment.** Phage

783 titres for phage DMS3vir over time across all experimental treatments (SA = *S. aureus*,

AB = *A. baumannii*, BC = *B. cenocepacia,* MC = microbial community), infecting either the PA14 WT or the CRISPR-KO strain as indicated by line type. Each data point represents a replicate, with lines following the mean and the error bars denoting 95% CI. Asterisks indicate a significant overall difference in phage density between the PA14 WT (n = 12 per timepoint) or CRISPR-KO clone (n = 6 per timepoint) (effect of *P. aeruginosa* clone; linear models: * $p < 0.05$).

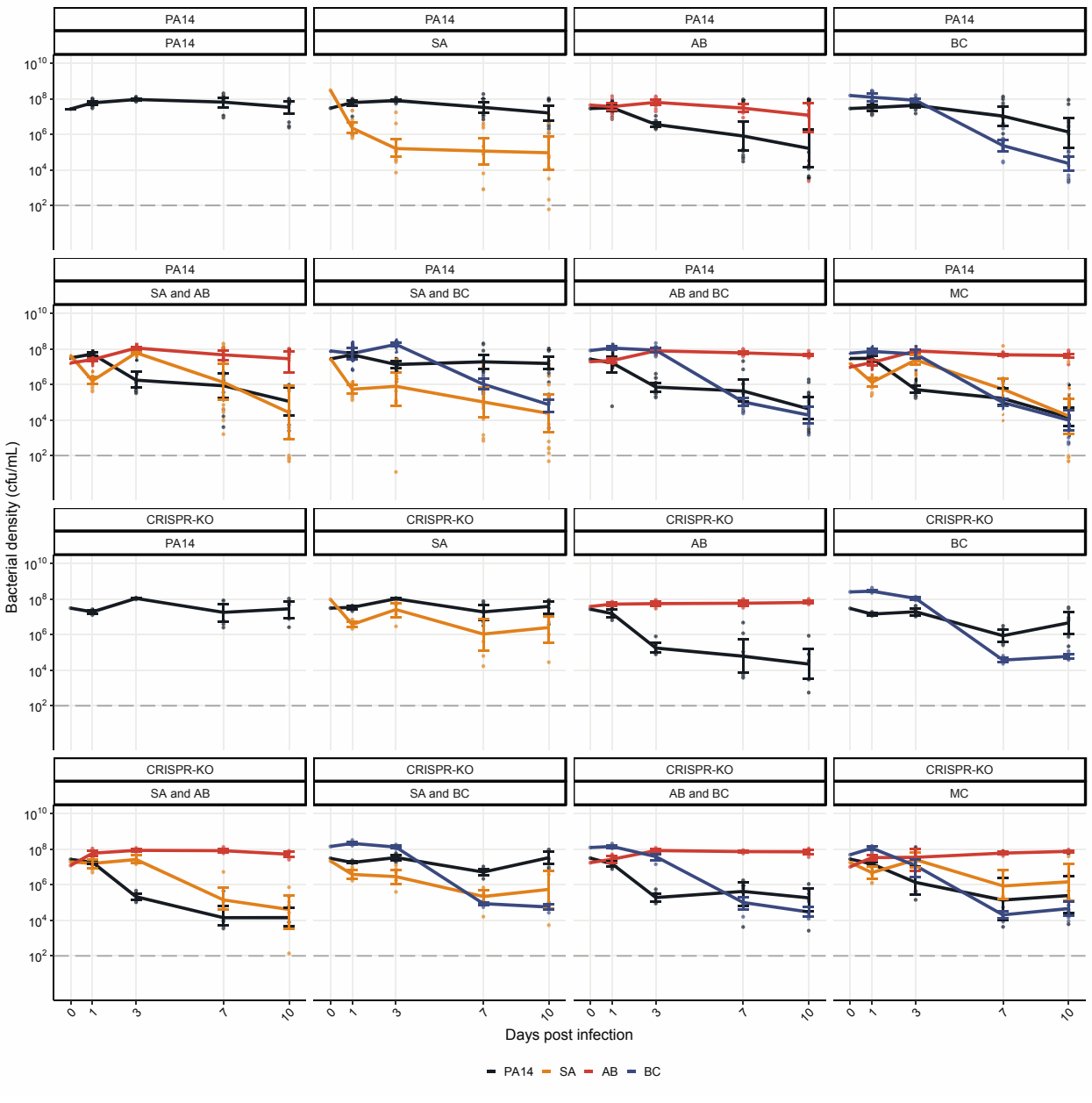

Supplemental Fig 5. Line plots of bacterial densities in the presence of phage. Showing the bacterial densities in cfu/mL over time for the PA14 WT and CRISPR-KO *P. aeruginosa* strains, and **b** the other microbial community species (SA = *S. aureus*, AB = *A. baumannii*, BC = *B. cenocepacia*, MC = Microbial community) in the presence of phage DMS3vir. Dashed horizontal line at 10^2 cfu/mL marks the threshold of reliable detection

where the qPCR results indicate the bacteria has gone or is close to extinction from a population. Data are mean ± 95% CI.

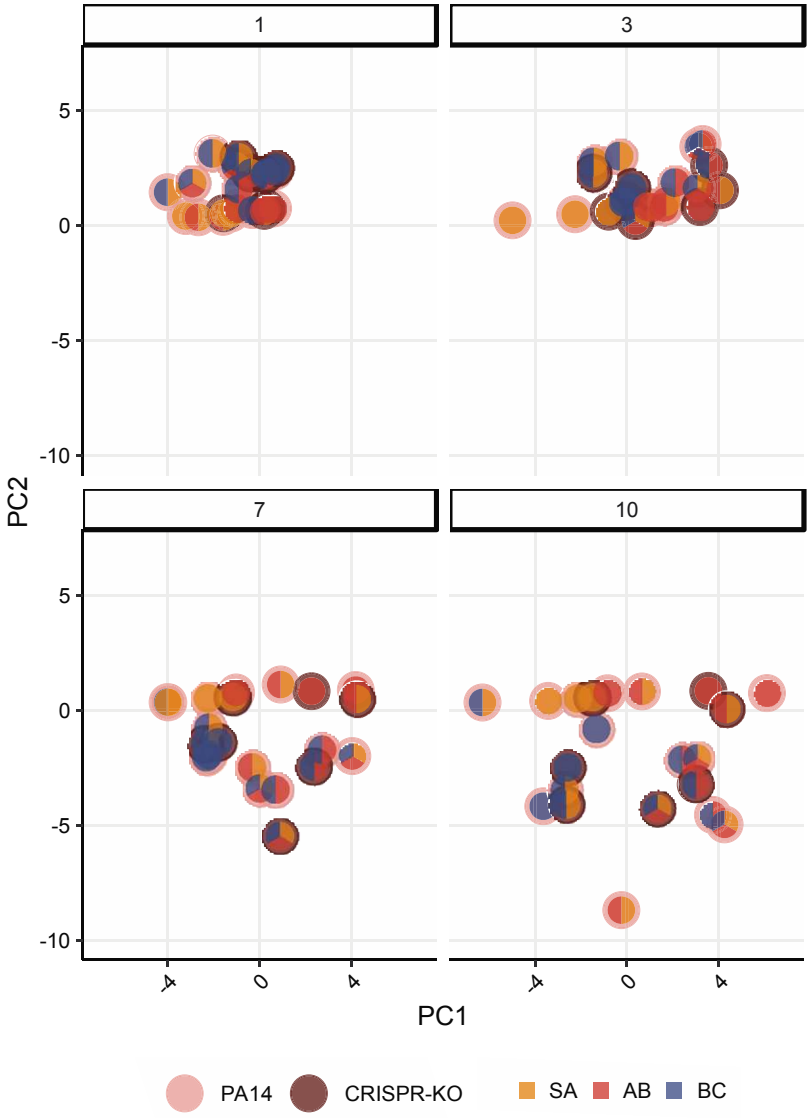

Supplemental Fig 6. Ordination plots in the presence of phage. PCA ordination of relative bacterial abundance in the presence of phage DMS3vir, with grid layouts separated into days post phage infection. Outer circle colour indicates which PA14 clone

804 is present in the population, while inner circle indicates community composition (SA = *S.*
805 *aureus*, AB = *A. baumannii*, BC = *B. cenocepacia*).
806

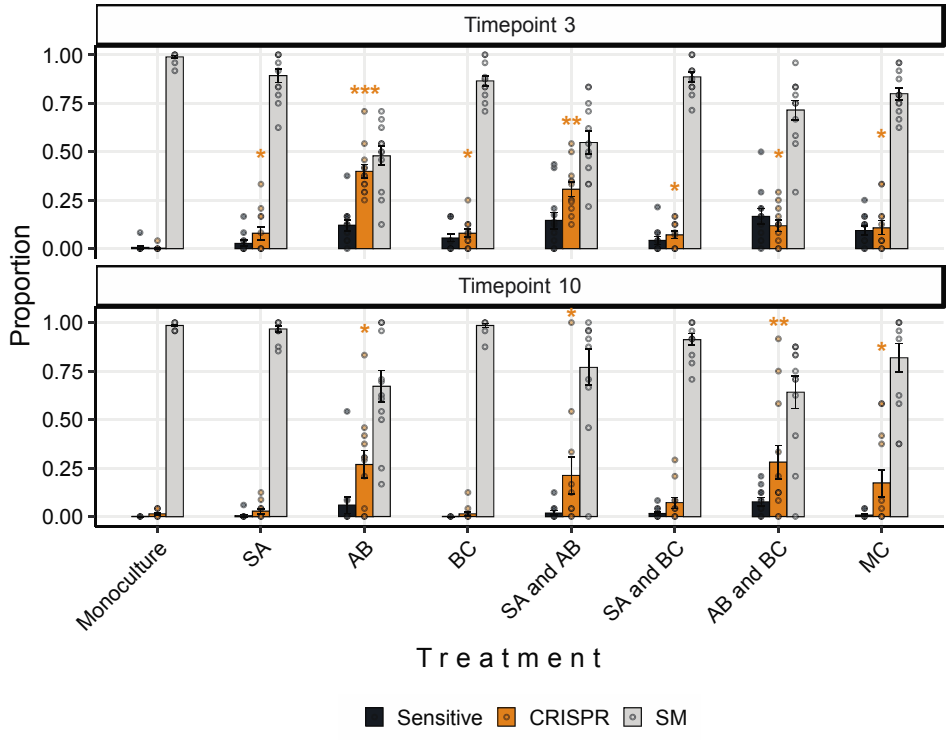

807

808 **Supplemental Fig 7. Interspecific competition affects the proportion of evolved**
809 **CRISPR-based phage resistance.** Proportion of *P. aeruginosa* PA14 WT at timepoints
810 3 and 10 that evolved phage-resistance either through surface modification (SM) or
811 CRISPR immunity, or which remained sensitive to phage DMS3vir when grown in
812 monoculture or different polycultures (SA = *S. aureus*, AB = *A. baumannii*, BC = *B.*
813 *cenocepacia*). Data are mean ± SE. Asterisks indicate a significant difference in
814 proportion of CRISPR immunity evolved when compared to the PA14 monoculture within
815 each timepoint (n = 12 per treatment) (generalised linear model, quasibinomial: * $p < 0.05$,
816 ** $p < 0.01$, *** $p < 0.001$).
817

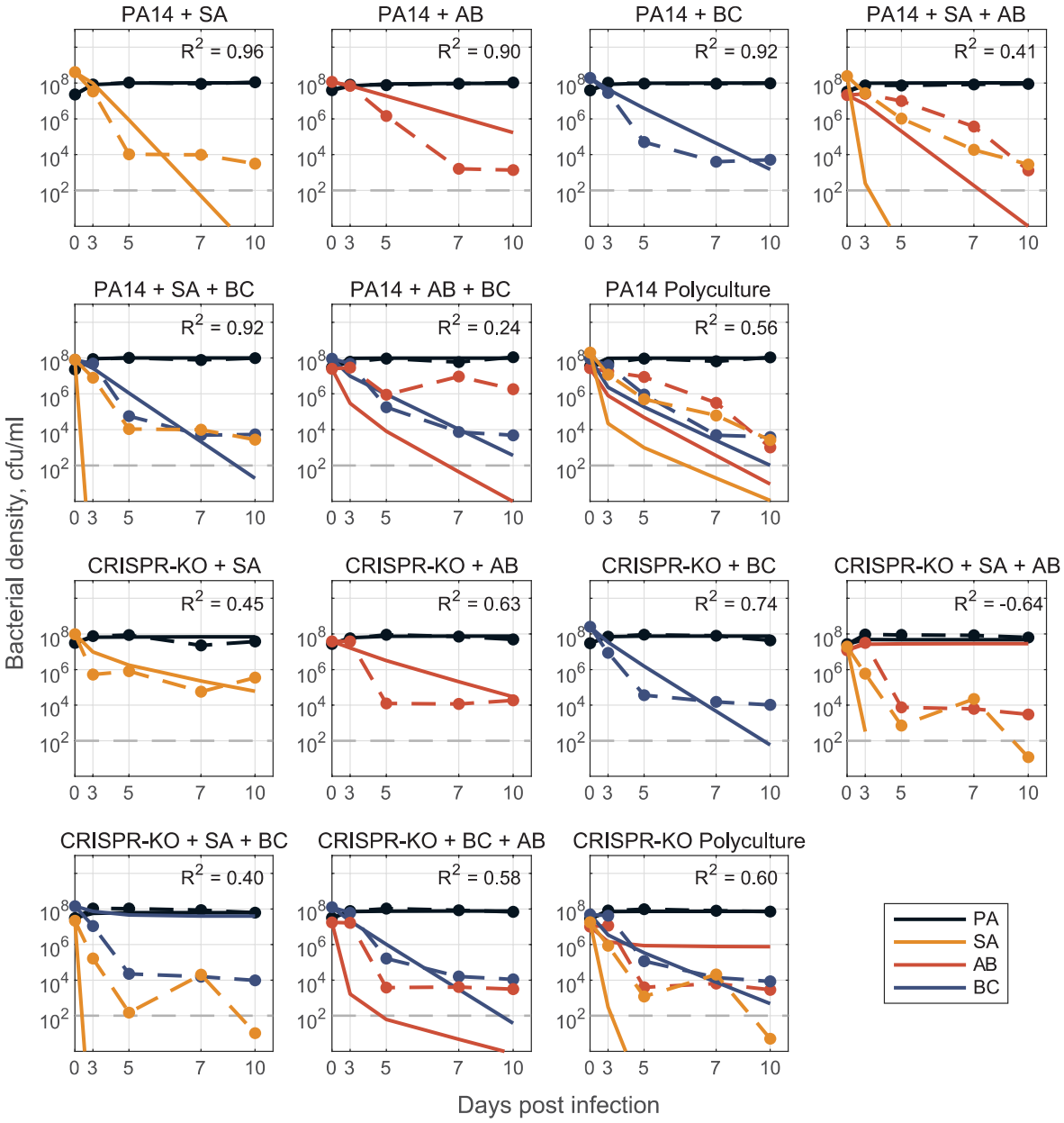

Supplemental Fig 8. Model from no phage data, trained on only pairwise experimental data. Model fit predictions for two-, three-, and full four species community dynamics (solid lines) compared to experimental data (dashed lines). Models were parameterized via optimization with least-squares to fit a system of ODEs (defined as a generalized Lotka-Volterra competition model with n species, where n=1,2,3,4). We parameterize the models via fitting of 1- (for growth rates r_i) and 2- (for all possible

pairwise interaction coefficients $\beta_{i,j}\ \forall i,j = 1,2$) species dynamics and use the resulting coefficients to predict the 3- and 4-species community dynamics. For fitting co-culture data, growth rates r_i were fixed from mono-culture data and interaction parameters $\beta_{i,j}$ were all open. See Methods and Text S1 for a detailed description of mathematical modelling.

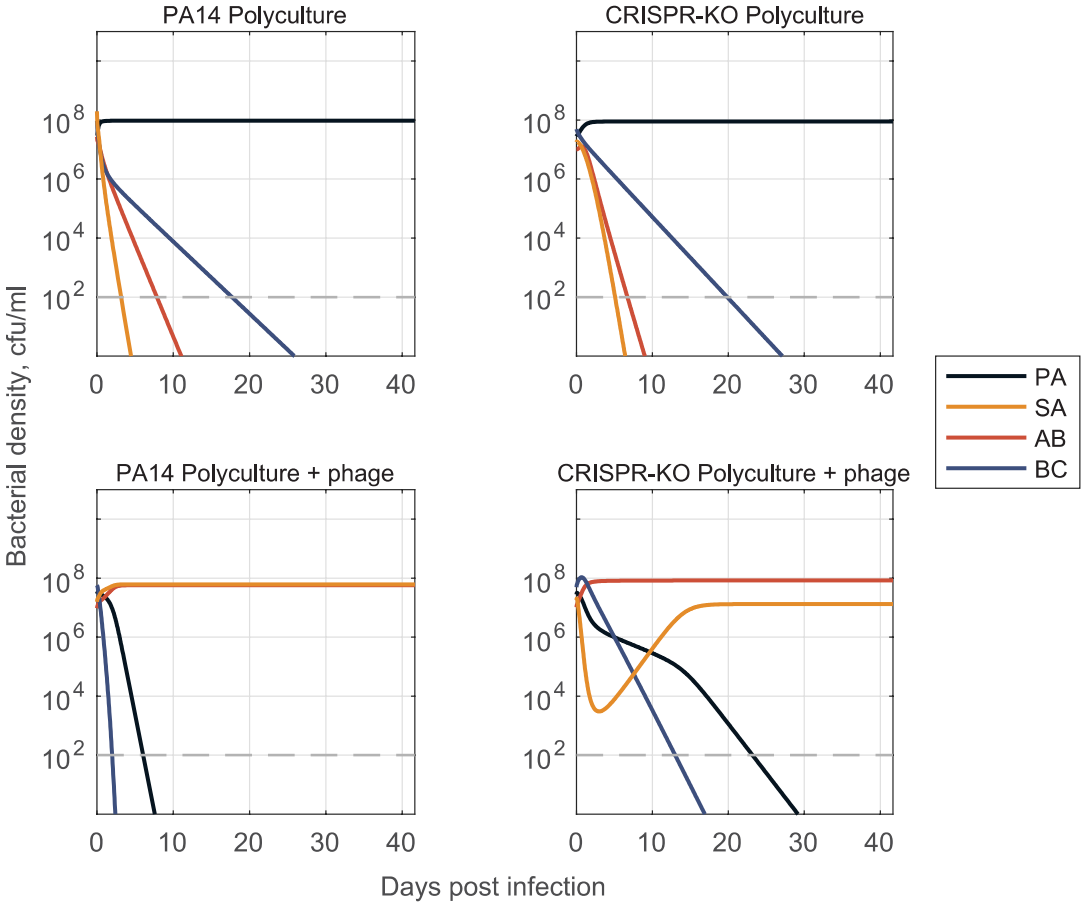

Supplemental Fig 9. Long time simulation of full community model shows shift in ecological outcomes given inclusion of phage. Simulation of the 4-species community gLV model over a long time scale reveals a qualitative shift in the outcome of the community when phage is present. In the absence of phage (top), *P. aeruginosa* is the dominant competitor and only surviving species. In the presence of phage (bottom), the

837 dominant competitor is eliminated, and we see competitive release of *A. baumannii* and
838 *S. aureus* – maintaining 2 of the 3 non-targeted species in the community. Growth and
839 interaction coefficients for simulation are from the model fits in Figures 7 and 8. For a
840 detailed description of model parameterization and simulation methods, see Methods and
841 Text S1.

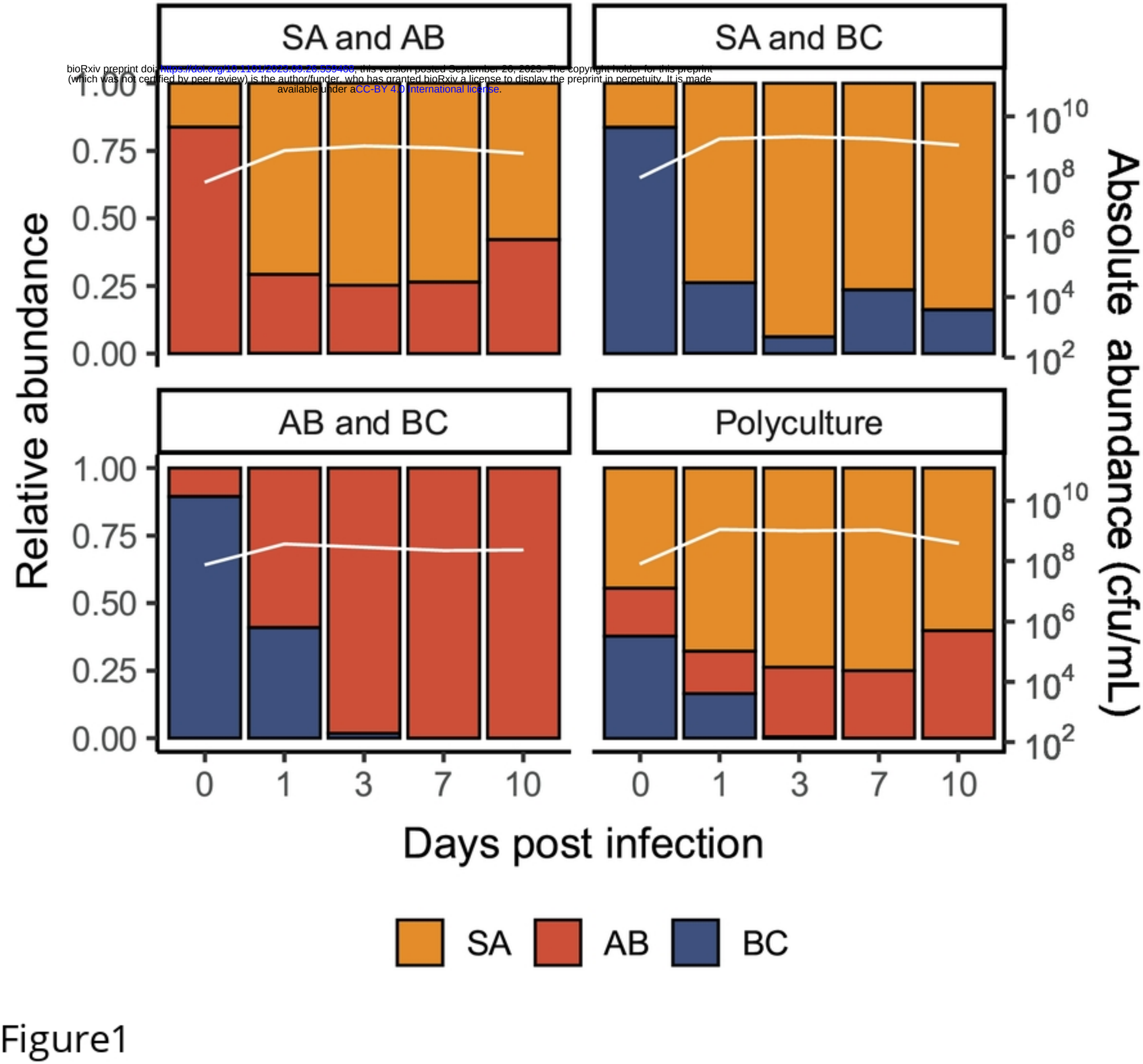

Figure1

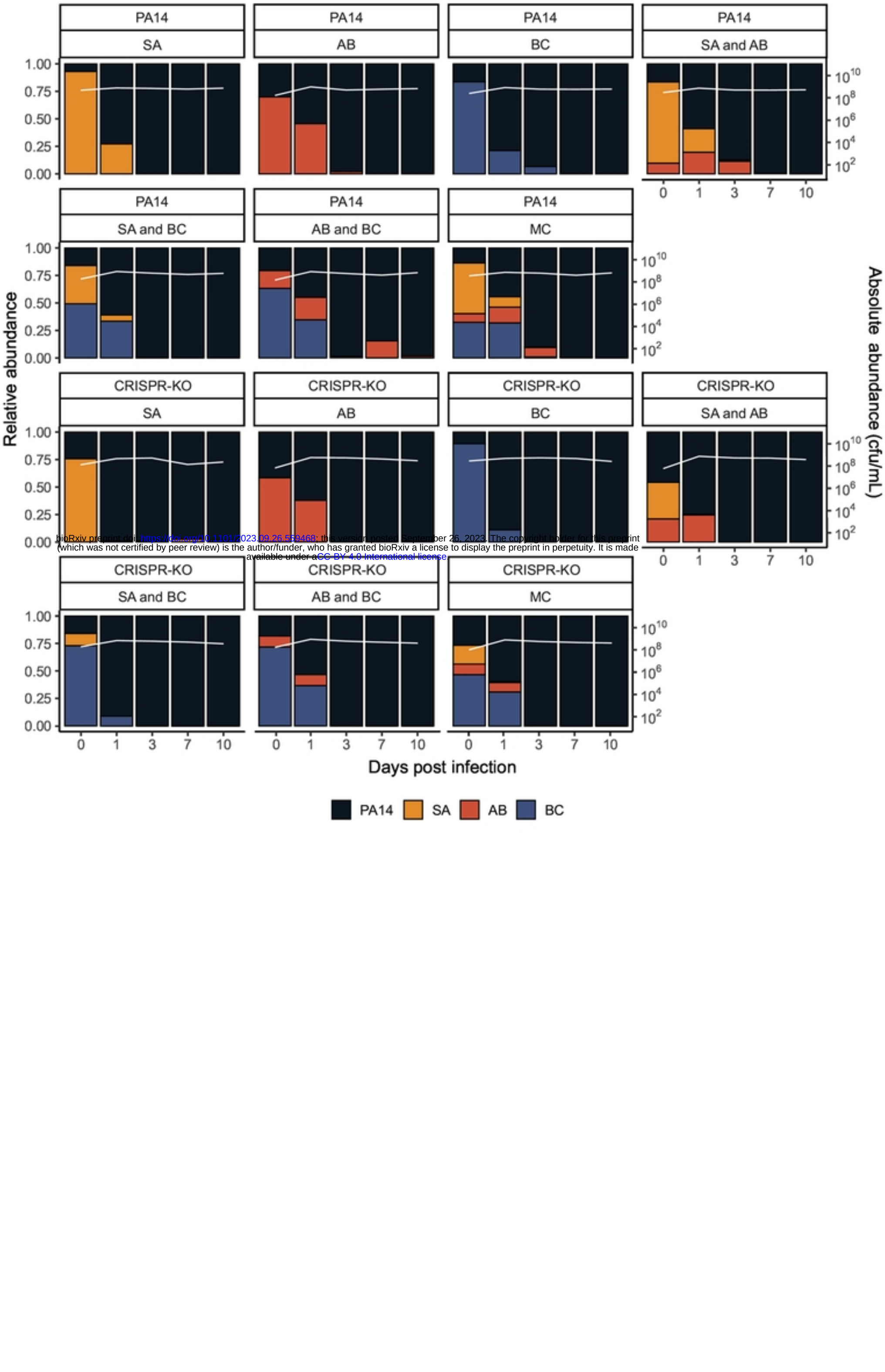

Figure 2

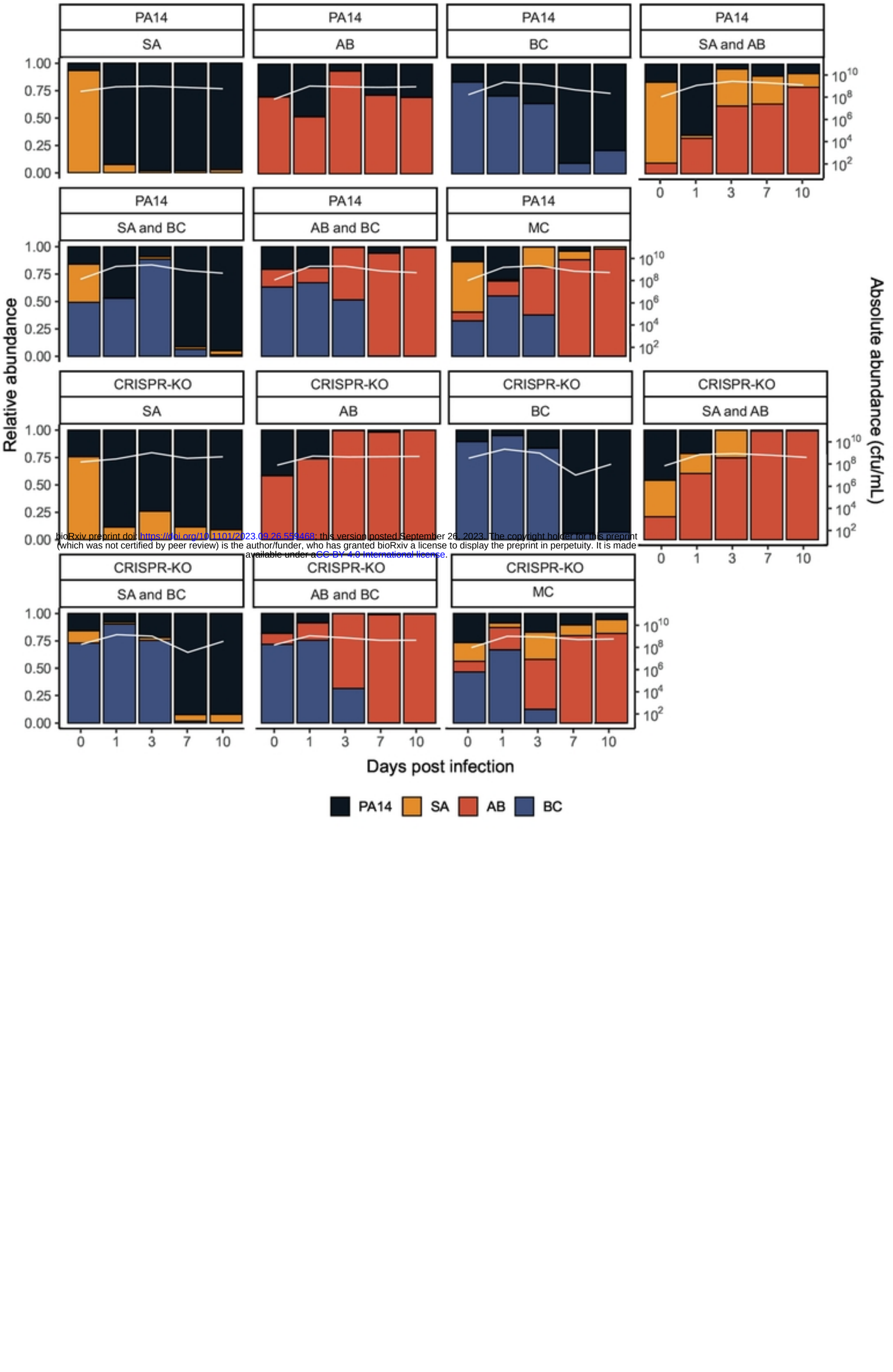

Figure 3

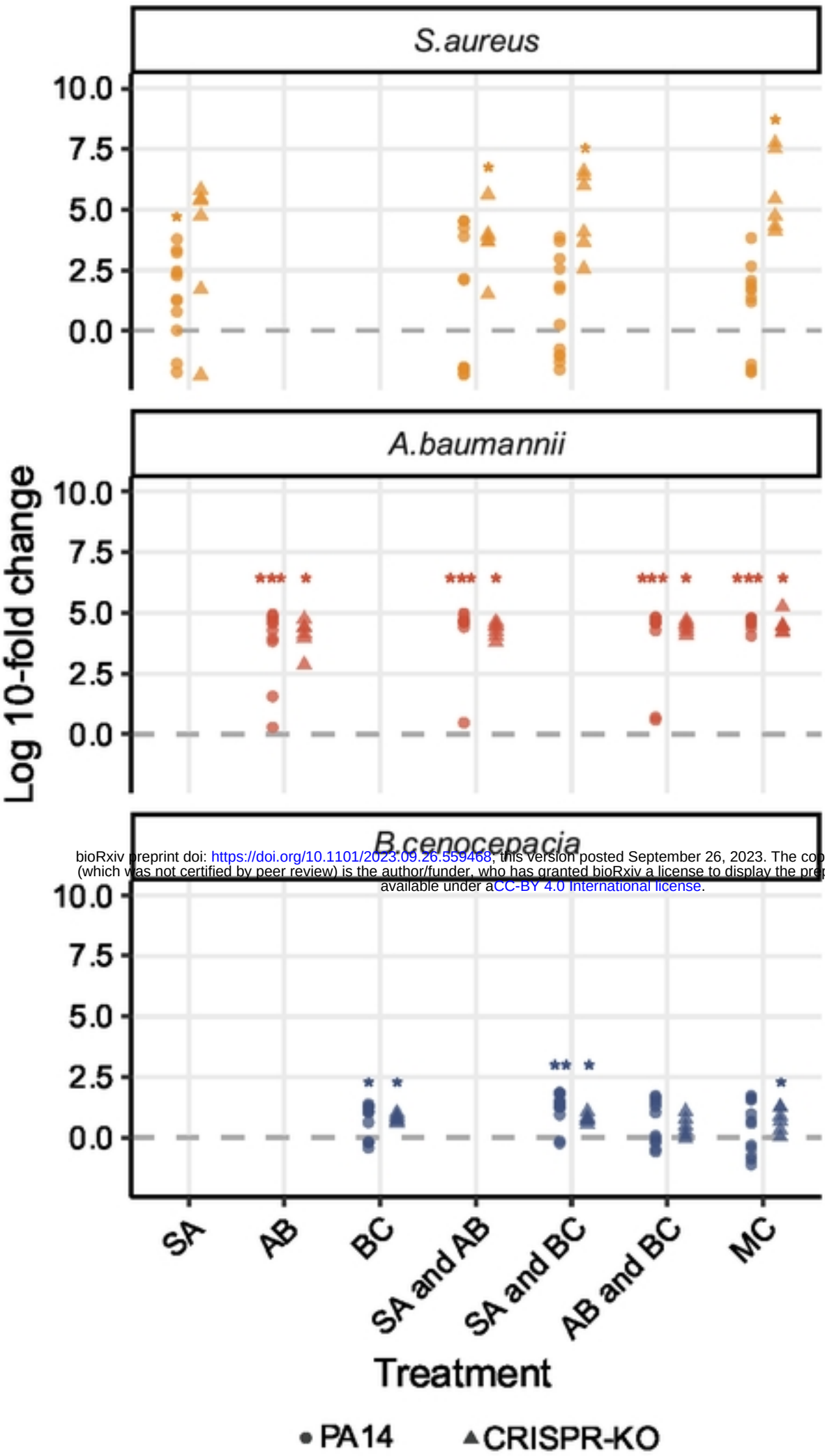

Figure 4

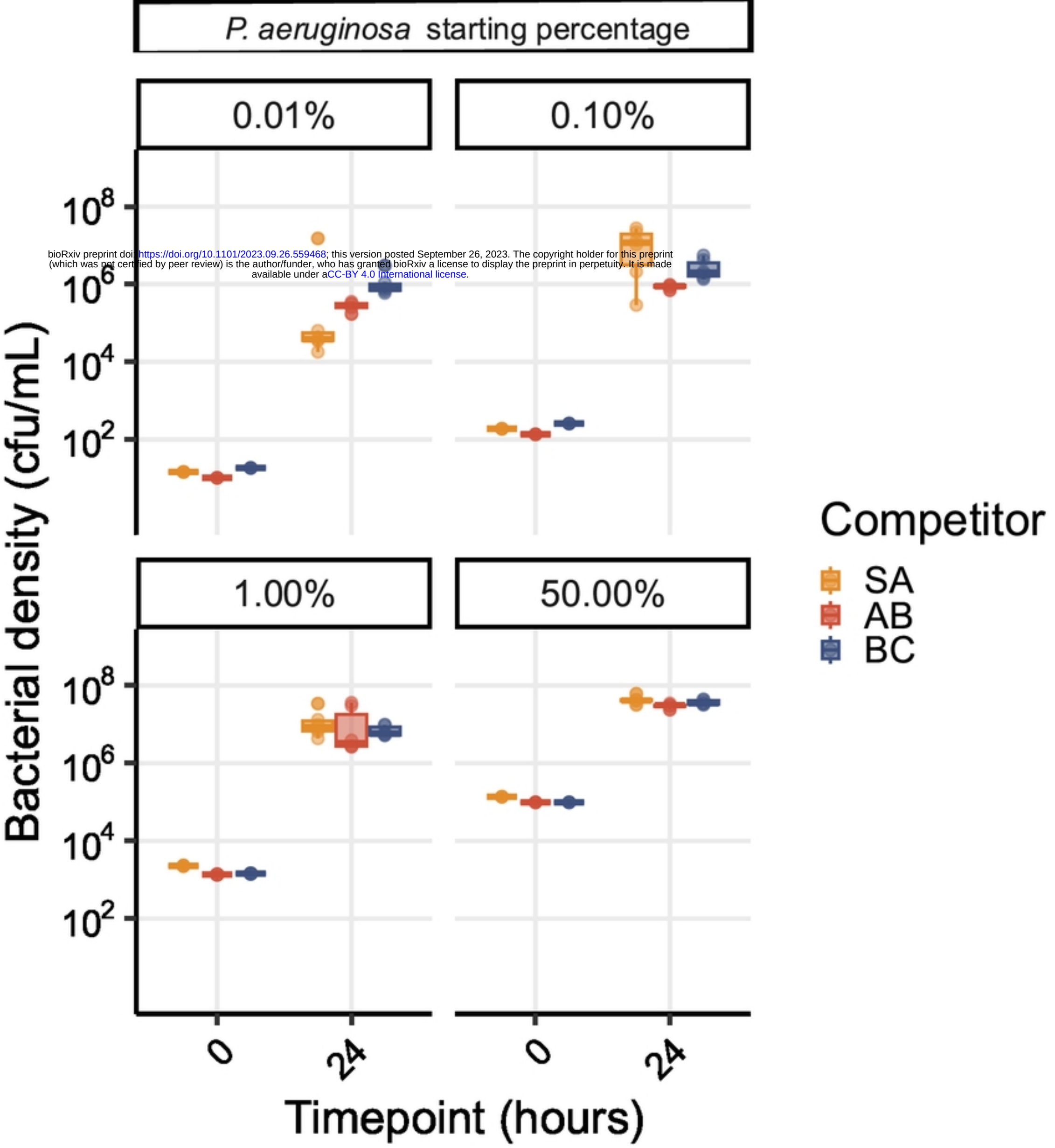

Figure 5

Figure 6

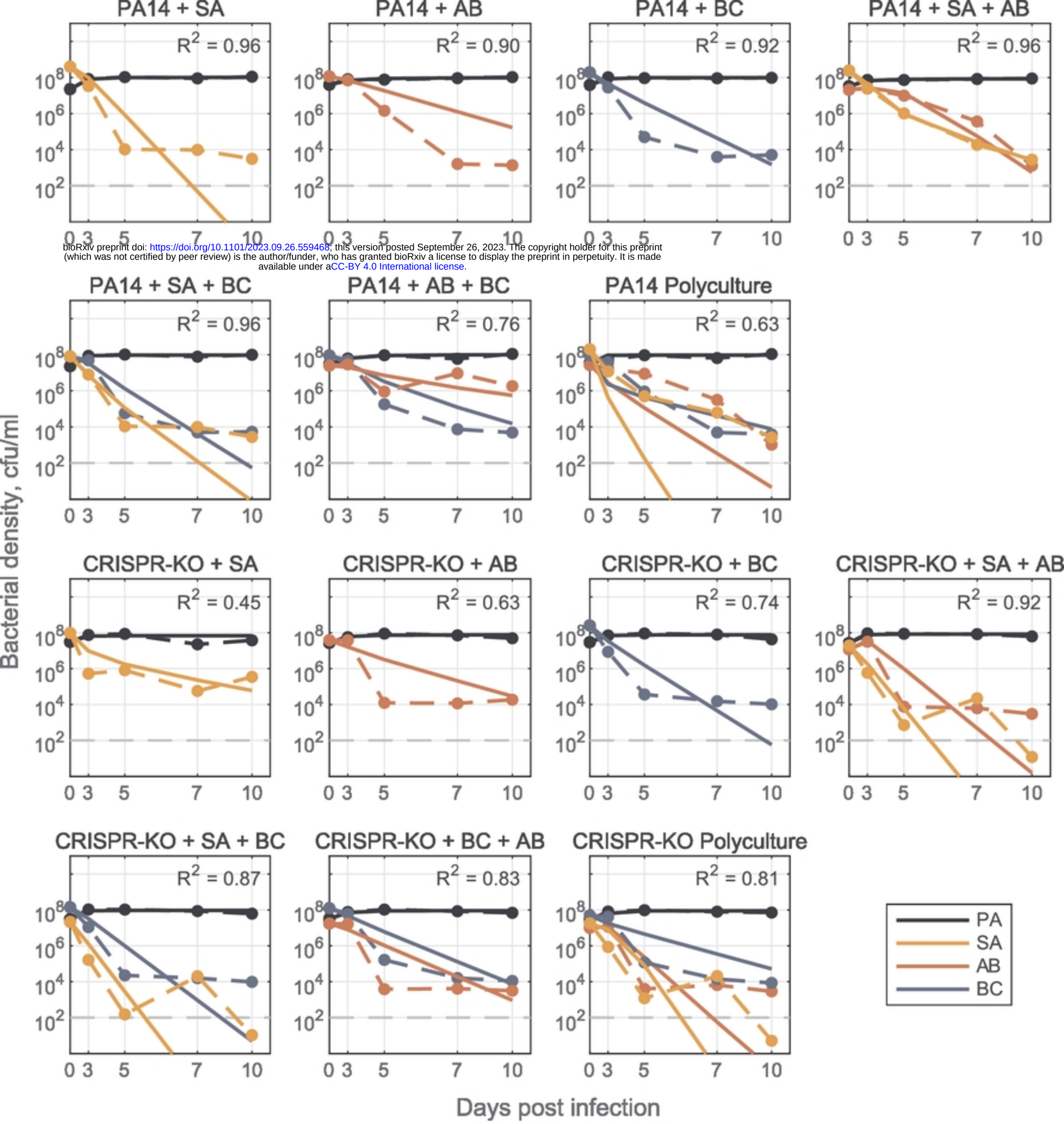

Figure 7

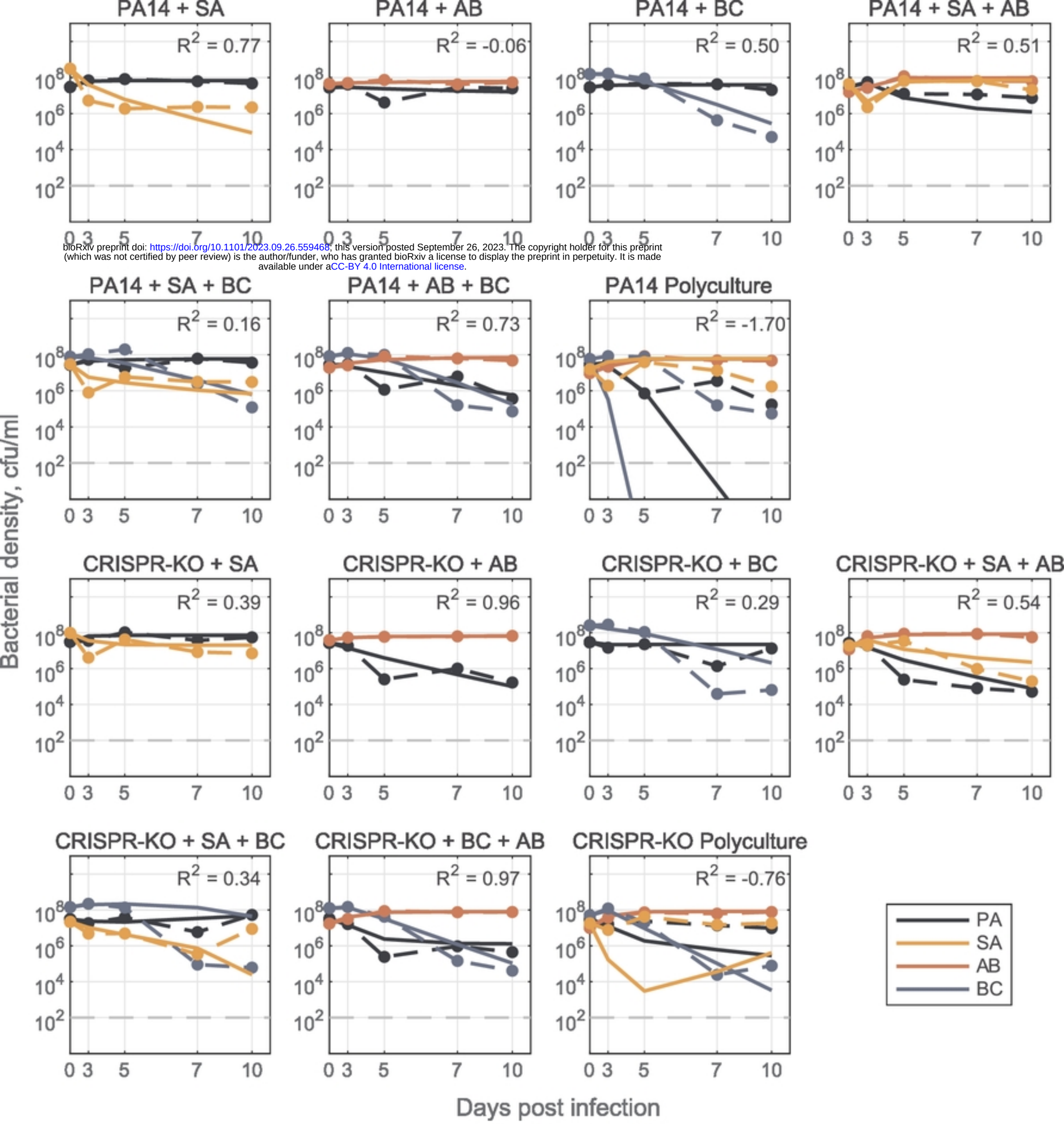

Figure 8

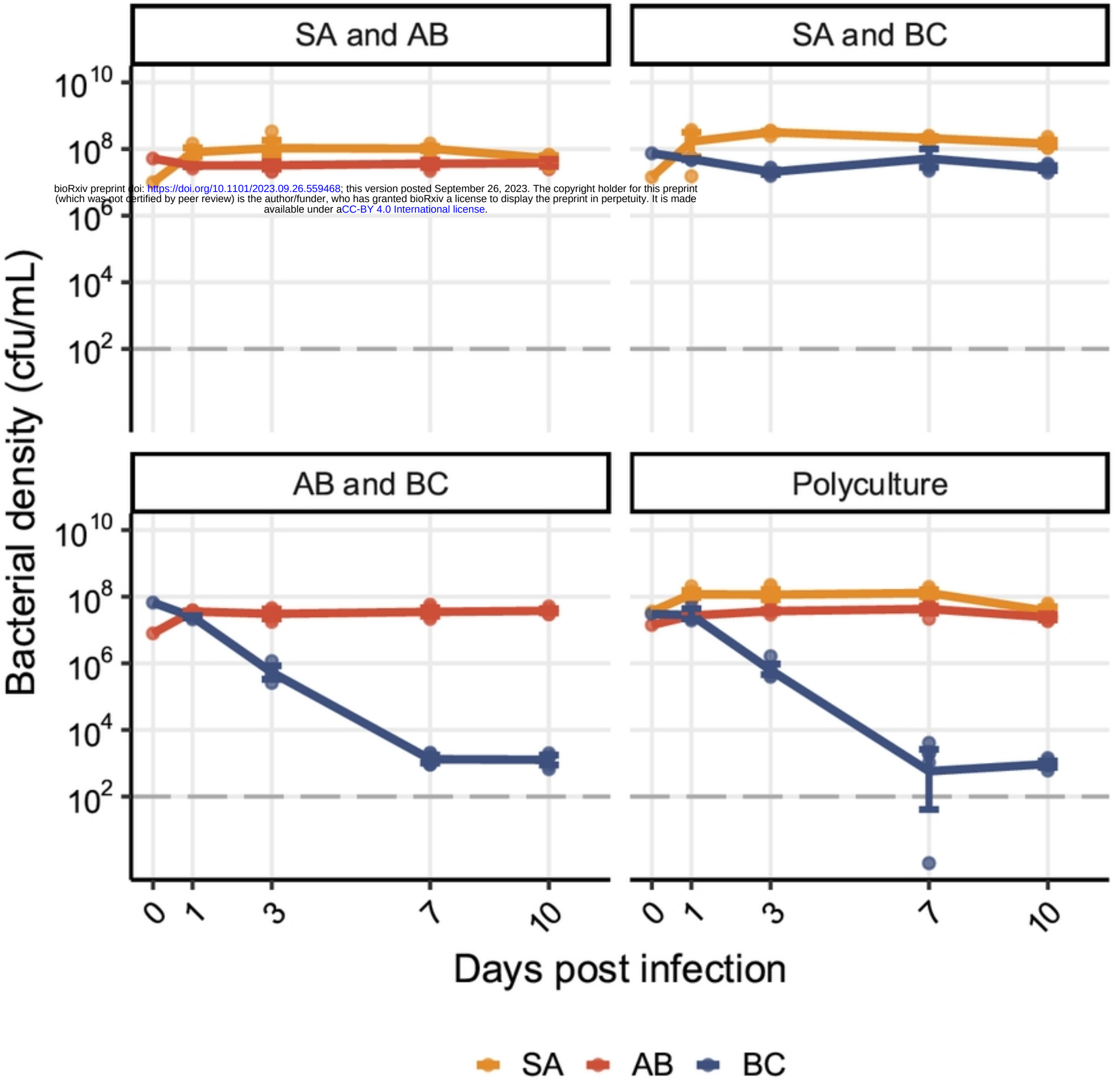

Figure S1

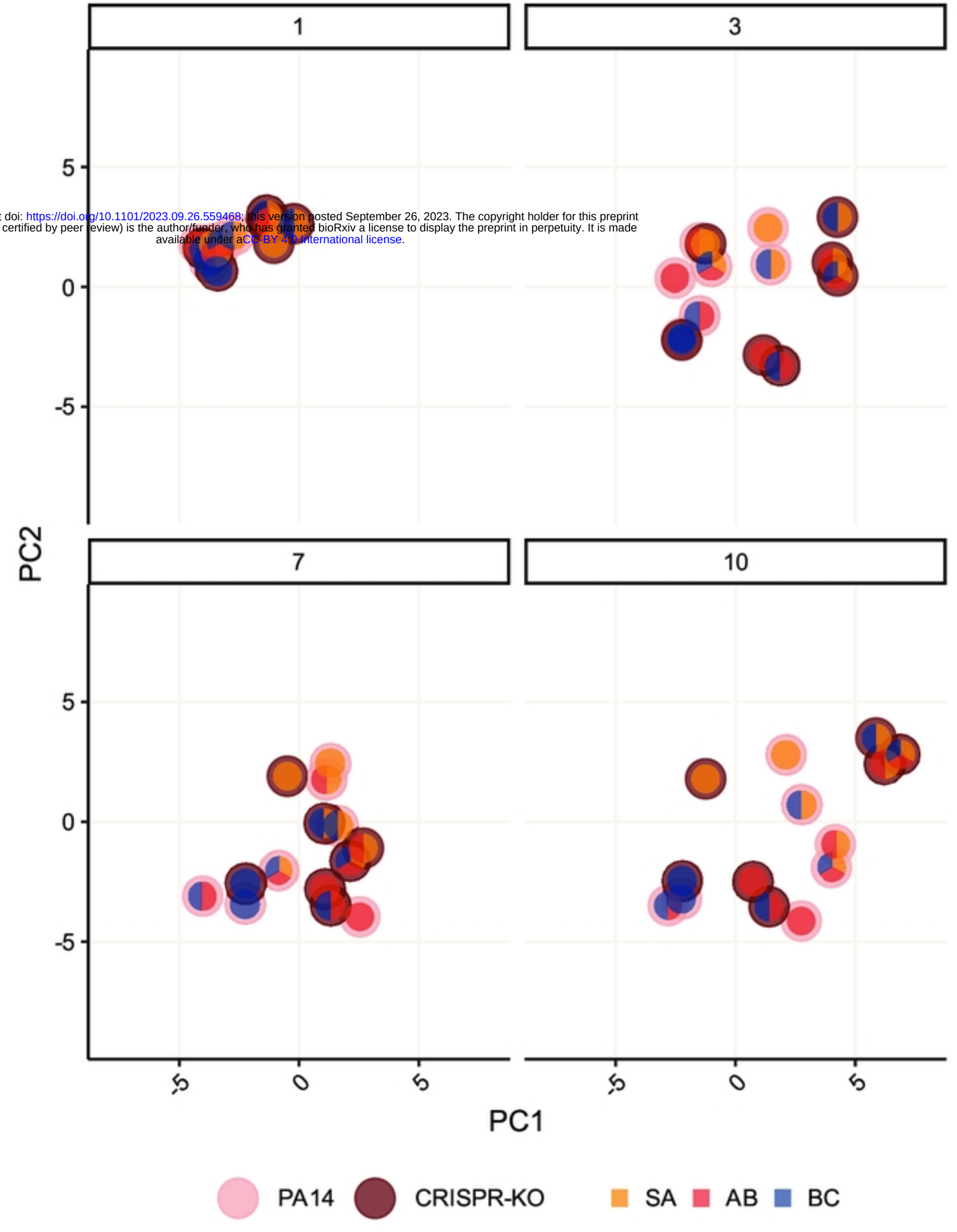

Figure S2

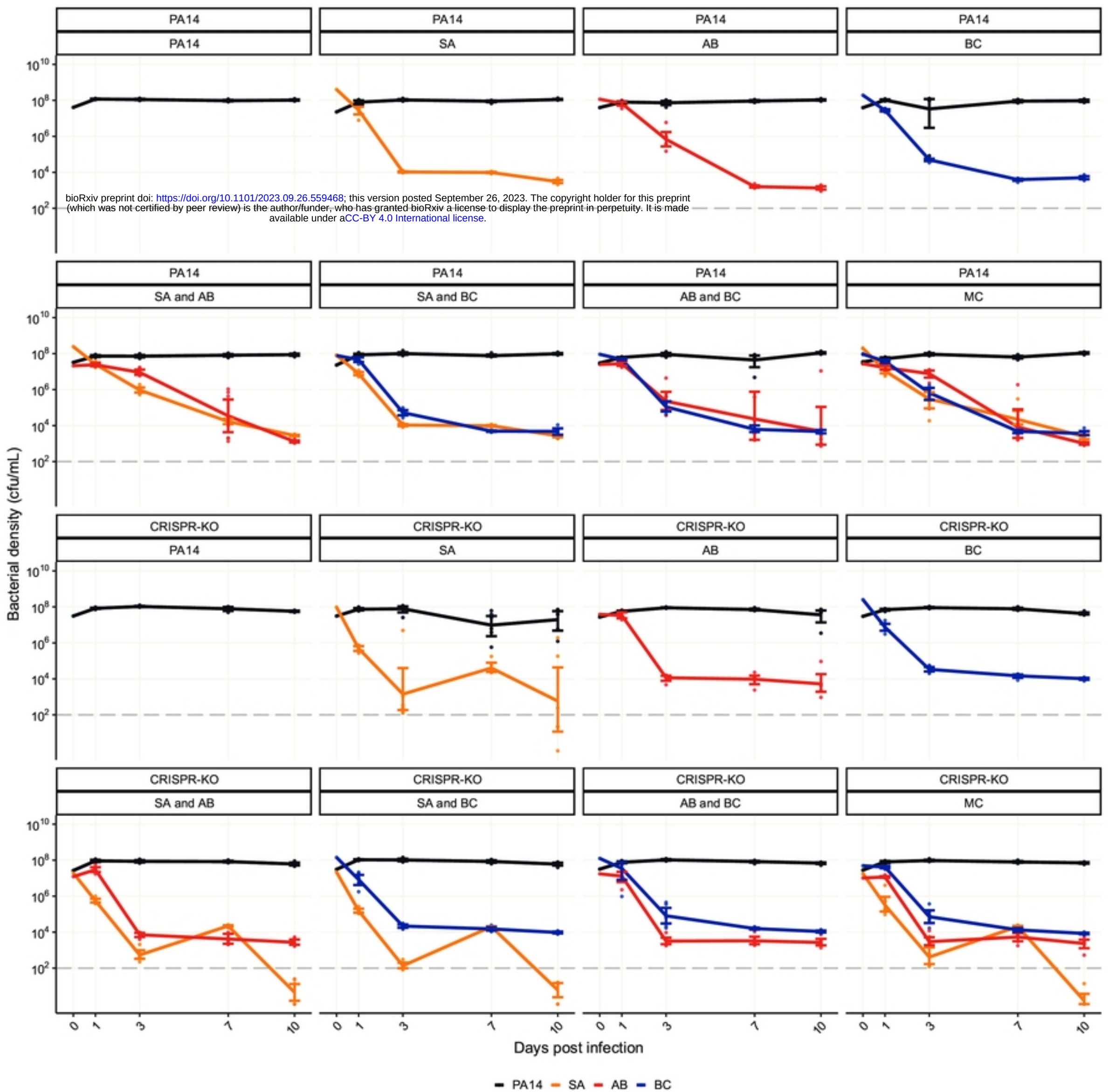

Figure S3

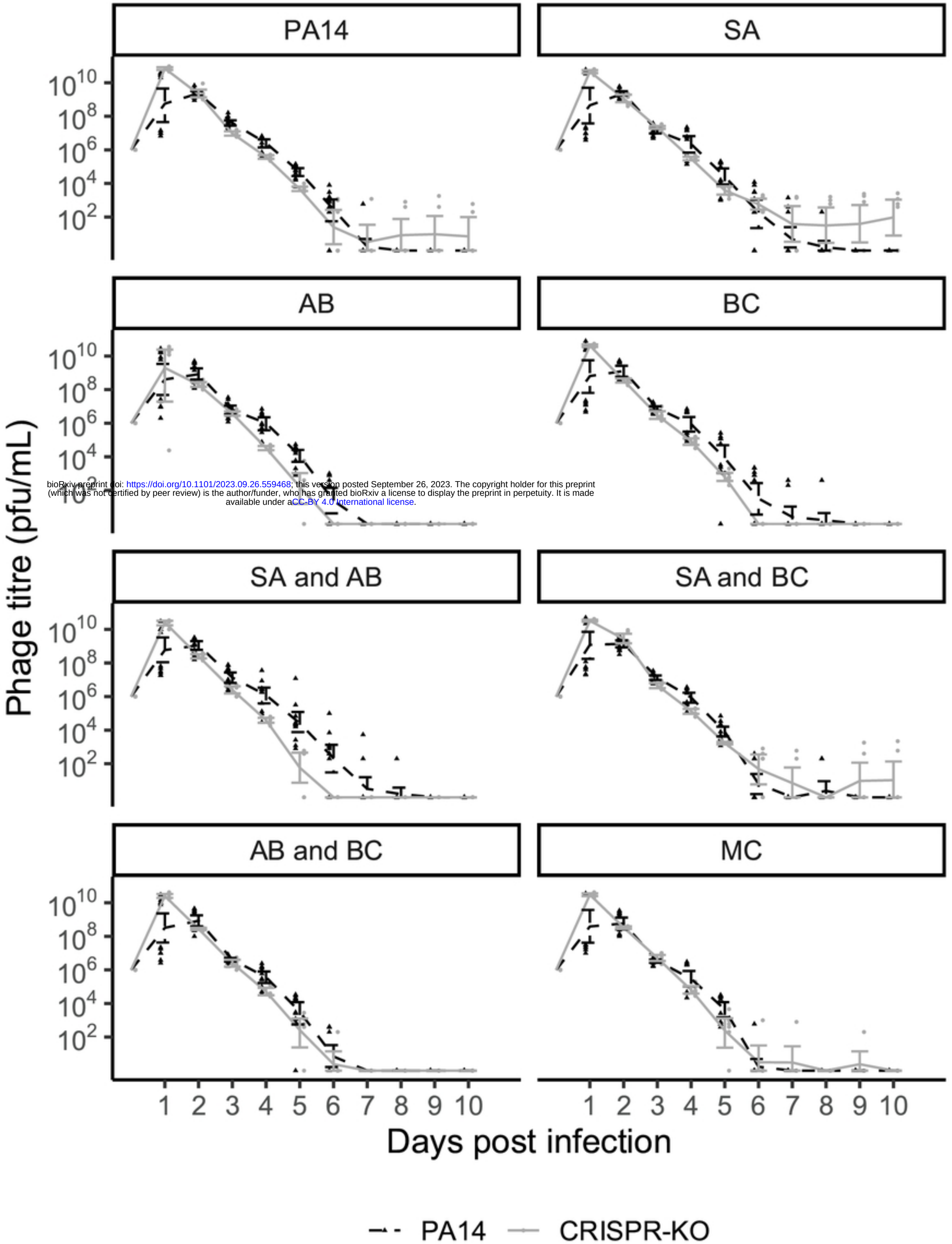

Figure S4

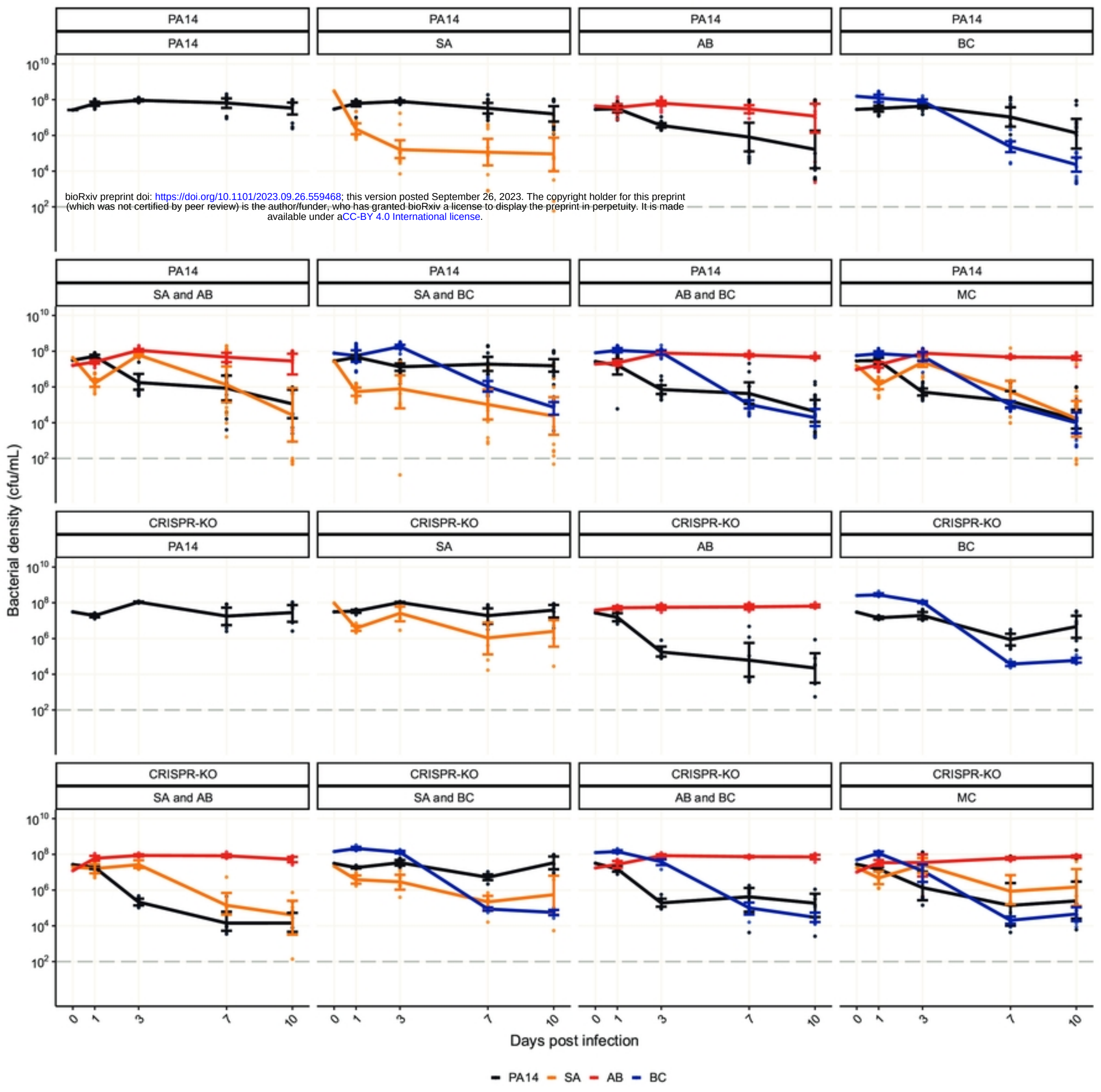

Figure S5

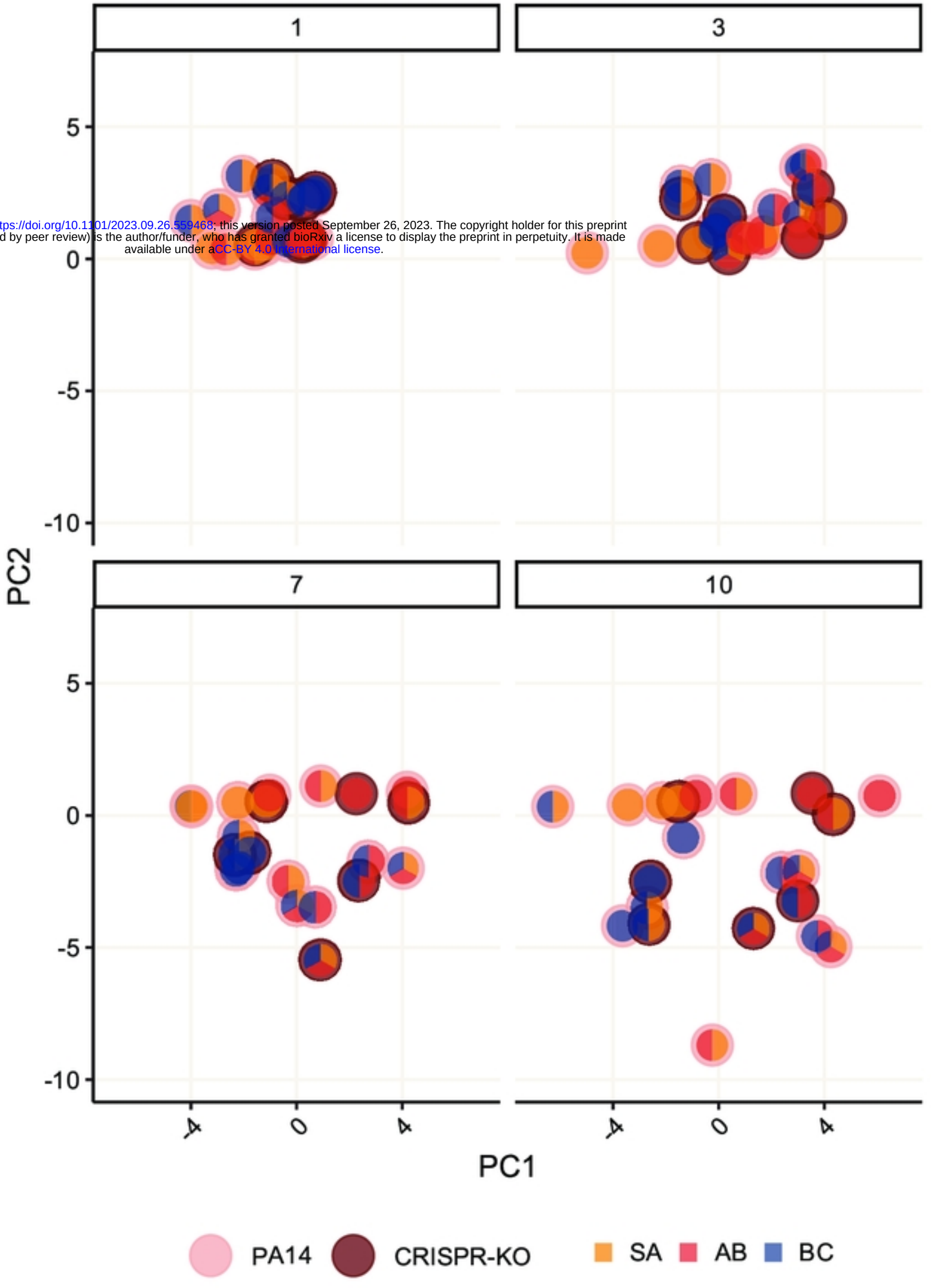

Figure S6

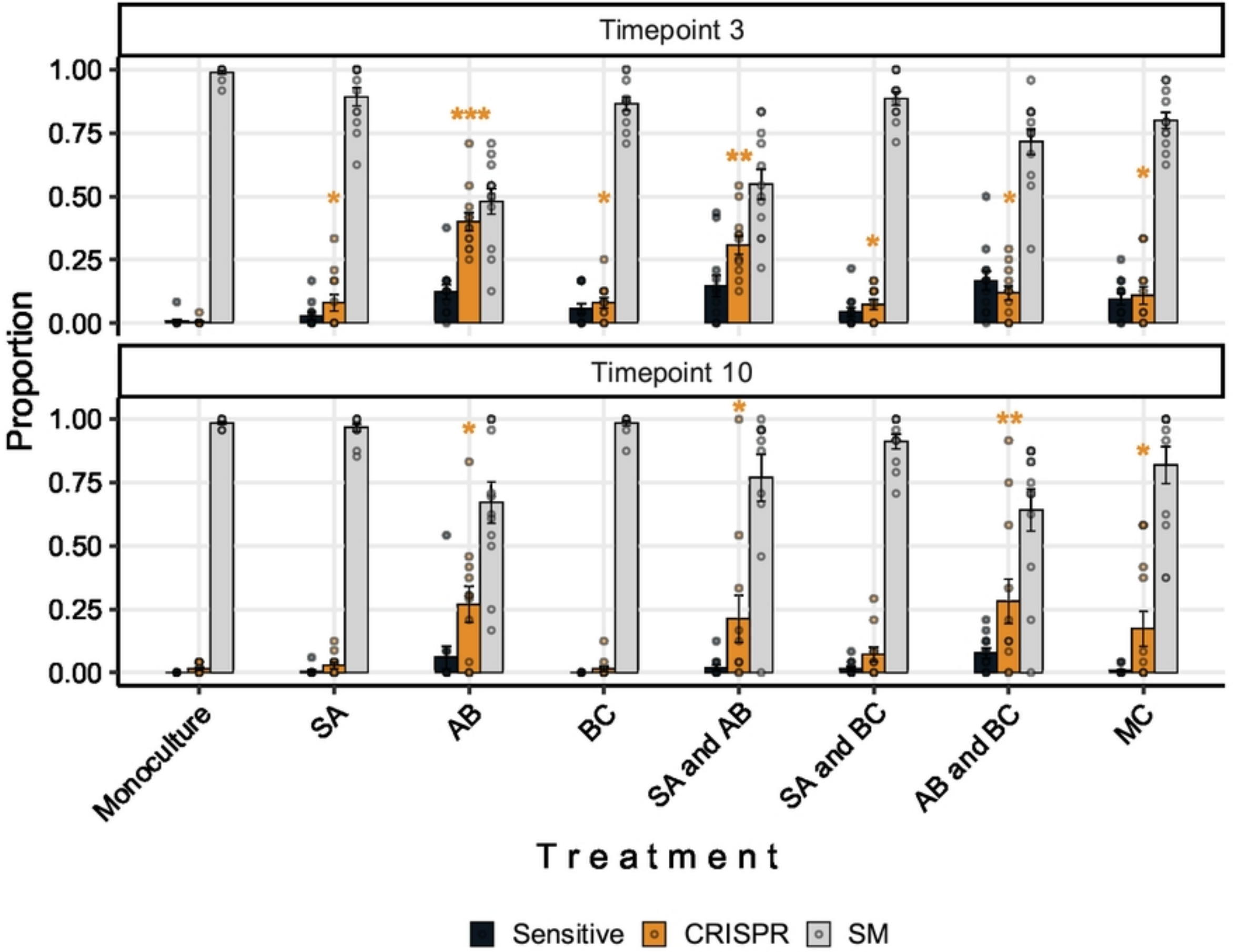
Timepoint 3
Timepoint 10
Proportion
1.00
0.75
0.50
0.25
0.00
Monoculture
SA
AB
BC
SA and AB
SA and BC
AB and BC
MC
Treatment
Sensitive
CRISPR
SM

Figure S7

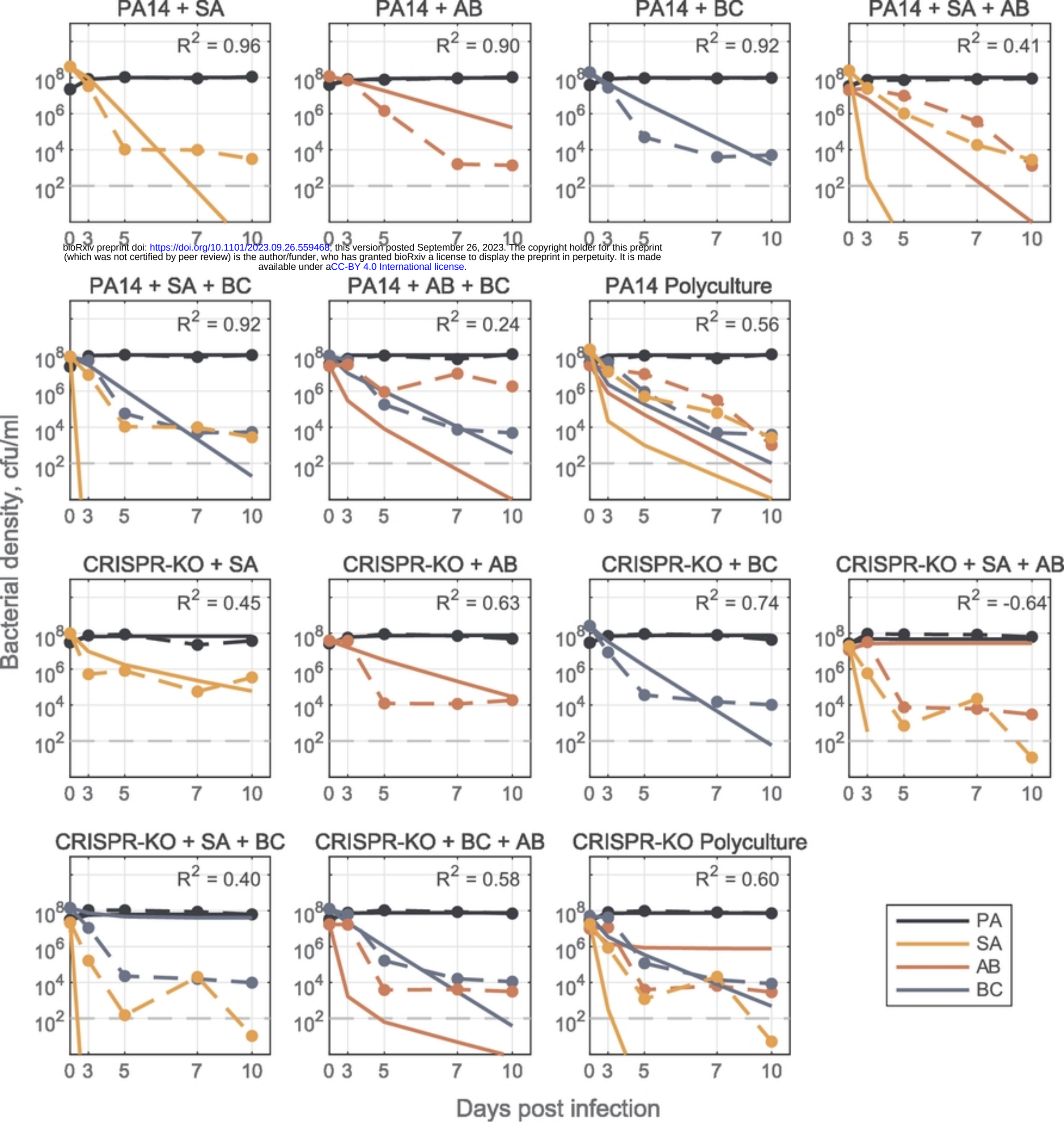

Figure S8

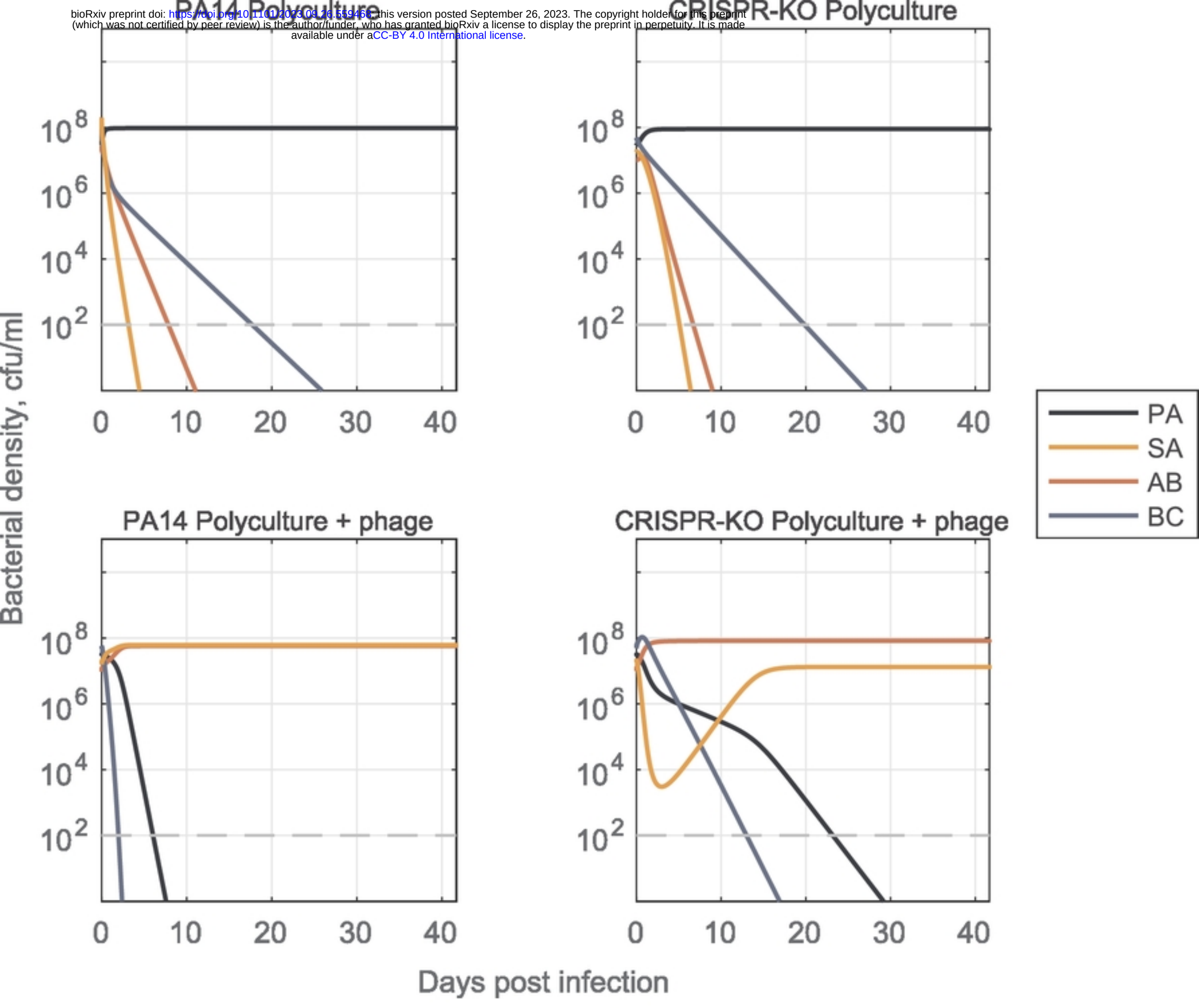

Figure S9